Microfacies and diagenesis of older Pleistocene (pre-last glacial maximum) reef deposits, Great Barrier Reef, Australia (IODP Expedition 325): A quantitative approach

Microfacies and diagenesis of older Pleistocene (pre-last glacial maximum) reef deposits, Great Barrier Reef, Australia (IODP Expedition 325): A quantitative approach

Eberhard Gischler*, Alex L. Thomas, Andre W. Droxler, Jody M. Webster, Yusuke Yokoyama and Bernd R. Schone

*Corresponding Author
Email: gischler@em.uni-frankfurt.de

Microfacies and diagenesis of older Pleistocene (pre-LGM) reefal deposits, Great Barrier Reef, Australia (IODP Expedition 325)

EBERHARD GISCHLER[1], ANDRÉ W. DROXLER[2], ALEX L. THOMAS[3], JODY M. WEBSTER[4], YUSUKE YOKOYAMA[5] and BERND R. SCHÖNE[6]

[1]Institut für Geowissenschaften, Goethe-Universität, 60438 Frankfurt am Main, Germany

[2]Department of Earth Science, Rice University, Houston TX 77251, USA

[3]Department of Earth Sciences, University of Oxford, South Parks Road, Oxford OX1 3AN, U.K.

[4]Geocoastal Research Group, School of Geosciences, University of Sydney, Sydney NSW 2006, Australia

[5]Atmosphere and Ocean Research Institute, University of Tokyo, Kashiwa Chiba 277-8564, Japan

[6]Institut für Geowissenschaften, Gutenberg-Universität, 55128 Mainz, Germany

ABSTRACT

During IODP Expedition 325, thirty-four holes were drilled along five transects in front of the Great Barrier Reef of Australia thereby penetrating some 700 m of reefal deposits of the late Pleistocene (postglacial; largely 20-10 kyrs BP) in water depths from 42-127 m. In seven holes, drilled in water depths of 42-92 m at three transects, older Pleistocene (older than last glacial maximum, pre-LGM, >20 kyrs BP) reefal deposits were recovered from lower core sections. In this study, facies, diagenesis, mineralogy, and stable isotope geochemistry of 100 samples from six of these holes, that contain pre-LGM deposits, were investigated and quantified. Lithologies are predominated by grain-supported textures. Based on quantitative analyses, eleven microfacies are delineated including mixed skeletal packstone and grainstone, mudstone-wackestone, coral packstone, coral grainstone, coralline algal grainstone, coral-algal packstone, coralline algal packstone, *Halimeda* grainstone,

microbialite, and caliche. Microbialites that are so common in the younger, postglacial deposits are very rare in older, pre-LGM core sections. In the pre-LGM deposits of holes M0032A and M0033A (>20 kyrs BP), marine diagenesis prevails. Holes M0042A and M0057A, which exhibit the oldest ages (>169 kyrs BP), predominantly show meteoric diagenesis. Holes M0042A, M0055A, and M0056A (>30 kyrs BP), and a horizon in the upper part of hole M0057A, exhibit both marine and meteoric diagenetic features, however, only one pore-water change from marine to meteoric is recorded, in contrast to the expected changes in diagenetic environment inferred from sea level change history. Stable isotopes of oxygen and carbon are consistent with these findings as samples from holes M0032A and M0033A have largely positive $\delta^{18}O$ and $\delta^{13}C$ values, whereas samples from holes M0042A and M0057A exhibit negative values. Holes M0055A and M0056A are intermediate, with slightly positive $\delta^{13}C$ ratios, and negative $\delta^{18}O$ values. Type and intensity of meteroric diagenesis appears to be controlled both by age and depth, *i.e*., time available for diagenetic alteration, and reflects the relationship between reef deposition and sea-level change.

KEYWORDS Great Barrier Reef Environmental Changes, Integrated Ocean Drilling Program, Expedition 325, Pleistocene, pre-LGM, facies, diagenesis

INTRODUCTION

Knowledge of facies, paleoecology, diagenesis, and age of late Pleistocene reefs is based on studies of the classic outcrops in New Guinea (Chappell, 1974; Pandolfi, 1996), Barbados (Mesolella, 1967; Jackson, 1992), the Red Sea (Gvirtzman & Friedman, 1977; Dullo, 1987, 1990; Strasser *et al*., 1992), and south Florida (Stanley, 1966). Subsurface or borehole studies in Pacific atolls (Quinn, 1991; Camoin *et al*., 2001; Braithwaite and Camoin, 2011), the Bahamas (Kievman, 1998), south Florida (Multer *et al*., 2002), the Great Barrier Reef

(Braithwaite *et al*., 2004; Braithwaite and Montaggioni, 2009), Belize (Gischler *et al*., 2010), or New Caledonia (Montaggioni *et al*., 2011) have concentrated either on facies, chronology, or diagenesis of Pleistocene reefs and carbonate platforms. However, during most of these studies only qualitative data were acquired. The results of diagenesis studies in Pleistocene reefs were detailed and summarized in various articles and textbooks (*e.g.*, Bricker, 1971; Longman, 1980; Harris *et al*., 1985; Schroeder and Purser, 1986). Still, uncertainties and open questions exist and refer, *e.g*., to the differentiation of meteoric-phreatic and marine-burial diagenesis that produce similar diagenetic patterns (Melim *et al*., 1995). Another problem is the correlation of sea-level variation with petrography, *i.e*., the possible lack of diagenetic records during high-amplitude sea-level falls (Melim, 1996), or the irregular distribution of cements in Pleistocene sequences (Braithwaite and Montaggioni, 2009). The analyses of climate archives from massive scleractinian corals have provided new insights into Pleistocene climate variability at high resolution (Tudhope *et al*., 2001; Felis *et al*., 2004; Gischler *et al*., 2009). These, and chronologic investigations such as exact radiometric dating during the past ca. 500 kyrs by the U/Th method including thermal ionization mass spectrometry (TIMS; Edwards *et al*., 1986) are hampered by diagenetic alteration of original aragonite and high-magnesium calcite mineralogies in the meteoric realm. It is therefore important to have a good understanding of the diagenetic history of the reef material if these studies are to be performed.

Our knowledge of late Quaternary reefs that were established in greater water depth or deposited during sea level lowstands has remained limited. Exceptions are the studies in Barbados (Fairbanks, 1989), New Guinea (Chappell & Polach, 1991), and Tahiti (Bard *et al*., 1996; Camoin *et al*., 2007; Iryu *et al*., 2010) that covered the time window back to the LGM and beyond, and produced almost complete postglacial sea-level curves (Bard *et al*., 1996, 2010). Interestingly, postglacial reefs of Tahiti and Australia were built largely by

microbialites (Westphal *et al*., 2010; Seard *et al*., 2011; Webster *et al*., 2011). Possibly, rapid sea-level rise created relatively open coralgal frameworks that offered habitat for microbes; rapidly changing environmental conditions potentially favored microbial accretion. With these aspects in mind, the material of IODP 325 to be studied here represents a unique opportunity to quantitatively investigate facies and diagenesis in reefs from lower sea levels in the late Quaternary (Fig. 1; Webster *et al*., 2011), and, in this case, those that reach back beyond the last glacial maximum (pre-LGM).

STUDY AREA

The Great Barrier Reef of Australia is the largest modern barrier reef system (Hopley *et al*., 2007). It is over 2,000 km long; the Queensland shelf behind the reef tract has widths of up to 220 km (Fig. 1). Results from studies on prominent reef settings around the world support the contention that major barrier reefs are geologically young features and only initiated during the late Pleistocene (mid-Brunhes, about 0.5 Ma). Marshall and Davies (1984) established that Holocene shallow-water reefs in the southern Great Barrier Reef developed on top of last interglacial reefs of marine isotope stage (MIS) 5 some 120 kyrs BP. Observations of the International Consortium for Great Barrier Reef Drilling (2001) suggest that the central Australian Great Barrier Reef (GBR) was established at approximately 600 kyrs BP. Abundant reef accretion started during MIS 11, approx. 400 kyrs BP (Webster & Davies, 2003; Braithwaite *et al*., 2004). Similar results were obtained in other barrier reef locations further afield such as for the Florida Reef Tract (Multer *et al*., 2002), for the New Caledonia barrier reef (Cabioch *et al*., 2008; Montaggioni *et al*., 2011), and for the Belize Barrier Reef (Droxler *et al*., 2003; Mazzullo, 2006; Gischler *et al*., 2010). One explanation for the development of thriving barrier reefs is the onset of 100-120 m, high-amplitude, eccentricity-driven sea-level fluctuations during the mid-Brunhes (about 0.5 Ma) that also contrasts with

the overall sea-level lowering trend since the onset of the northern Hemisphere glaciation about 2.7 Ma (Lisiecki and Raymo, 2005; Miller et al., 2005).

IODP Expedition 325 "Great Barrier Reef Environmental Changes" had three major objectives including the reconstruction of deglacial sea level (20-10 kyrs BP), the estimation of variability of sea surface temperature and sea-level change on reef growth including drowning, and the high-resolution quantification of paleoclimatic change from coral skeletons. According to preliminary chronology (Webster *et al*., 2011; Yokoyama *et al*., 2011), the majority of the 34 holes drilled on 5 transects cover the time period of about 20-10 kyrs BP. Postglacial sections appear diagenetically unaltered and comprise coralgal boundstone, coralgal-microbial boundstone, skeletal grainstone/rudstone, and unconsolidated sand. However, sections older than LGM (>20 kyrs BP) exhibit a different variety of facies and a much more complex diagenetic evolution.

The five drill sites of IODP Expedition 325 include from north to south the Ribbon Reef area, Noggin Pass, and Hydrographer's Passage (Fig. 1). Holes were drilled in water depths ranging from 40-170 m, to the east of the Great Barrier Reef margin. The shelf margin is characterized by fifteen geomorphological features including submerged terraces, pinnacles, ridges, and channels (Abbey *et al*., 2011). These authors interpreted the features as fringing, patch, and barrier reefs as well as tidal channels that were largely formed during mid-late Pleistocene sea-level variation. The samples investigated here are from holes M0055A, M0056A, and M0057A drilled at Noggin Pass in water depths of 42-87 m and from holes M0032A, M0033A, and M0042A drilled at Hydrographer's Passage in water depths ranging from 51-92 m (Fig. 1; Table 1).

METHODS

One-hundred samples from six holes (M0032A, M0033A, M0042A, M0055A, M0056A, and

M0057A) recovered during IODP 325 were investigated with regard to facies, mineralogy, diagenesis, mineralogy, and stable isotope geochemistry of oxygen and carbon. Thin-sections (4x6 cm) of all samples were studied using a petrographic microscope and point-counter in order to study and quantify facies and diagenetic features (constituent particles, cements, primary and secondary porosity). Two-hundred points were counted per thin-section, i.e., the absolute error for a given component, cement, or pore space with an abundance of 50% would be 7%; for an abundance of 10% the error would amount to 4% (van der Plaas and Tobi, 1965). Staining with Feigl's solution, Titan Yellow, and Alizarine was used on representative samples in order to differentiate between common carbonate minerals such as aragonite, high-magnesium calcite, and low-magnesium calcite (Friedman, 1959). Relative amounts of carbonate minerals in all samples (bulk) were estimated by X-ray diffractometry using the method of Milliman (1974, p. 21-27). Stable isotope ratios of oxygen ($\delta^{18}O$) and carbon ($\delta^{13}C$) were measured in subsamples (60–120 μg) of powdered bulk samples, that were reacted with 100% H_3PO_4 at 72 °C, using a ThermoFinnigan MAT253 mass spectrometer with GasBench II, according to the method of Spötl and Vennemann (2003). Average internal analytical precision equaled 0.03 and 0.05‰ for $\delta^{18}O$ and $\delta^{13}C$, respectively. An in-house Carrara marble standard was used as a reference material ($\delta^{18}O$ = -1.91‰, $\delta^{13}C$ = 2.01‰; calibrated against NBS-19). Preliminary chronology for all holes was established, from core catcher material, prior to sampling of the core sections at the Onshore Science Party in Bremen, Germany, and by U-series and radiocarbon (^{14}C AMS) measurements (Webster *et al*., 2011). Four further U-series ages of core material (Table 1) were determined at the University of Oxford, UK (detailed chronologies of Expedition 325 material will be published elsewhere). Sedimentological, mineralogical, diagenetical, and geochemical data were analyzed statistically (correlation and cluster analyses) using the software PAST. In cluster analysis, Ward's algorithm was used as it produced the most meaningful results.

RESULTS

Microfacies

The majority of pre-LGM samples are skeletal packstones and grainstones (Figs. 2, 3; Table 2). The most common skeletal grains identified originate from, in decreasing abundance: coralline red algae, corals, benthic foraminifera, *Halimeda*, mollusks, and echinoderm skeletons, shells, and tests. Non-skeletal grains, almost exclusively peloids, are rare. Eleven facies were delineated based on a cluster analysis (algorithm: Ward's method) of the quantitative data (Fig. 4; Table 2). In order to characterize depositional facies, only abundance data of skeletal and non-skeletal components, microbialite and caliche features were included in the cluster analysis. Data on diagenesis, mineralogy, and geochemistry (Tables 3, 4) were excluded here. The eleven identified facies include mixed skeletal packstone, mixed skeletal grainstone, mudstone-wackestone, coral packstone, coral grainstone, coralline algal grainstone, coral-algal packstone, coralline algal packstone, *Halimeda* grainstone, microbialite, and caliche. Based on the cluster analysis, coralgal packstone and coralline algal packstone are subfacies, however, they are treated as individual microfacies here. No clear spatial patterns of microfacies distribution can be identified. Minor exceptions include *Halimeda* grainstone that is most common in hole M0042A, caliche that preferentially occurs in samples from hole M0056A, and microbialite that was only identified in hole M0056A. Results of the correlation analysis show that the abundances between certain components are statistically significant (Table 5). The abundances of the most common component coralline algae exhibits a negative correlation with those of *Halimeda* and a positive correlation with those of encrusting foraminifera (*Carpenteria* sp.). The abundances of coral and other components only show negative correlations. *Halimeda* fragments appear to occur preferentially with shells and tests of mollusks, benthic foraminifera, and echinoderms.

Abundances of mollusks, benthic foraminifera, echinoderms, and peloids are also positively correlated.

The eleven delineated microfacies are:

(1) Mixed skeletal packstone (msp).— This is the most abundant microfacies (Figs. 3g; 5a; 6f; 7e). It contains coralline algae, coral, *Halimeda*, benthic and encrusting foraminifera, and mollusks. Matrix reaches average values of 27%. Mean porosity in this microfacies is 16%. About 20% are marine and meteoric cements.

(2) Mixed skeletal grainstone (msg).— This microfacies is characterized by the same skeletal components, with coralline algae more clearly predominating as compared to the previous microfacies (average abundance >10%). Matrix only reaches a mean value of 2%. Porosity averages 20% and cements 37% (Figs. 6f; 7d).

(3) Mudstone-wackestone (mw).— A mean abundance of 62% matrix characterizes this microfacies. Benthic foraminifera and *Halimeda* are the most common skeletal components. Porosity is lower as compared to grain-supported textures and averages 6.5%. Cements make up 5.2%.

(4) Coral packstone (cp).— This microfacies is clearly dominated by coral fragments that average 34.5% abundance. Fragments of coralline algae have the second highest abundance. Matrix has a mean value of 23%; cements average 17.8%. Porosity averages at 8%.

(5) Coral grainstone (cg).— Close to 40% of this microfacies are coral fragments (Figs. 3f; 7c). Likewise, the portion of marine and meteoric cement reaches a mean value of 40%. Porosity amounts to 16% on average.

(6) Coralline algal grainstone (cag).— Coralline algae occur with a mean abundance of 22% (Figs. 3a; 5b; 7a, f). Benthic foraminifera are common with a mean abundance close to 7%. Cements (30%) and porosity (20%) make up half of the volume of this microfacies.

(7) Coral-algal packstone (cp).— Fragments of coral and coralline algae dominate equally in this microfacies and reach a mean abundance of 38% (Fig. 7b). Matrix and cements have average values of 17% and 24%, respectively. Mean porosity is close to 10%.

(8) Coralline algal packstone (cap).— This microfacies has similarities with the previous one, however, the ratio between coralline algae and corals is different. Coralline algae reach a mean abundance of 29% and corals only 3%. Benthic and encrusting foraminifera average 11% (Fig. 5c). Matrix has an average value of 21%. Cements and porosity make up 17% and 11% on average, respectively.

(9) *Halimeda* grainstone (hg).— Close to two thirds on average of this microfacies are well-preserved flakes of the alga *Halimeda* (Figs. 3c; 6a-e). Benthic foraminifera, corals, and coralline algae are common. Cements make up 27.5%. The porosity averages 12%.

(10) Microbialite (m).— Microbialite was identified in hole M0056A (Figs. 3h; 5d). It resembles layered postglacial microbialites in post-LGM reef deposits of the same cores and those described from postglacial reefs of Tahiti (Westphal *et al.,* 2010; Seard *et al*., 2011). The microfacies exhibits more or less regular changes in color from light brown to buff. In thin-section, the facies appears dense (mean porosity 5%; cement 17%) and fine-grained, with an irregular laminated texture. Mottled or thrombolitic texture is rare. Skeletal fragments can be seen interspersed into the microbialite (Fig. 5d).

(11) Caliche (c).— Caliche is a secondary diagenetic product, however, as it is not uncommon in pre-LGM sections and was analyzed in thin-section, it is listed here. Caliche may be seen already in small hand specimens based on brownish and/or reddish staining, irregular lamination, and dissolution surfaces (Figs. 3a, d; 5e, f). In hole M0056A at about 20 m depth, caliche phenomena are developed over several meters along core. In thin-section, the rock appears fine-grained and moderately dense with a mean porosity of 14%. Brown lamina, mottled and clotted textures, and micro-brecciation is common (Fig. 5e). Rhizoliths (Fig. 3a)

and diagenetic geopetals (Fig. 5f) may be seen occasionally. Cement makes up 21% on average. Skeletal fragments are interspersed in this facies. The calcite content ranges from 50-75%.

Diagenesis

Thin-section analysis has shown that a variety of carbonate cement morphologies and compositions, neomorphism, and features such as dissolution and caliche occur within the pre-LGM samples collected during IODP 325 (Figs. 5-7; Tables 2, 3). On average, cements reach an abundance of 22.7%. Porosity has a mean value of 13.6%.

Micrite envelopes are observed occasionally in holes M0042A and M0056A (Figs. 6a, b, d; 7b, e). In these cores, they can be best seen around mollusk shells and fragments of coral skeletons. Micrite envelopes are most abundant in hole M0057A. In this core, they often mark the outlines of former aragonite or high-magnesium calcite particles that have been replaced by blocky low-magnesium calcite. In a number of examples, micrite envelopes also occur on the outer rims of isopachous acicular (needle) cement crusts (Fig. 6a, d).

Aragonitic acicular (needle) cement is most abundant in holes M0032A and M0033A (Fig. 5a; Fig. 6a, d). It is found occasionally in the upper investigated sections of the other holes M0042A, M0055A, M0056A, and M0057A. Needle cement usually forms isopachous crusts; individual crystals are up to 200 μm long and less than 5 μm um wide. Botryoidal aragonite cement is rather rare in the samples investigated and occurs only in the upper parts of holes M0032A and M0042B (Fig. 7c). Individual botryoids get up to 750 μm thick.

Peloidal high-magnesium calcite cement is observed throughout holes M0032A and M0033A as well as occasionally in the upper investigated sections of holes M0042A, M0055A, and M0056A (Fig. 5a; Fig. 6b). Preferentially, this cement occurs within primary pores of skeletal grains. Peloids are 20-30 μm in diameter, consist of a microcrystalline core,

and are surrounded by small (10-30 μm), dentate crystals. Microcrystalline cement consists of high-magnesium calcite, appears dark brown under the microscope, and is occasionally found in all cores. Crystals have diameters of 2-3 μm.

Features of dissolution are found in all hole sections except for M0032A and M0033A. Skeletal components of gastropods, corals, *Halimeda*, and bivalve shell fragments are preferentially dissolved thereby leaving mouldic porosity (Fig. 5b, c). Coralline algae and benthic foraminifera are observed to have been dissolved, however, to a much lower degree. It appears that aragonite components are affected by dissolution to a larger degree when compared to calcitic shells, tests, and skeletons. Dissolution is in many cases accompanied by neomorphism of aragonite and high-magnesium calcite to blocky low-magnesium calcite. Occasionally, preferentially in high-magnesium calcite precursors, traces of the original grain texture may still be recognized after grain alteration. Neomorphism is most common in holes M0057A and M0042A.

Blocky low-magnesium calcite cement is very common in holes M0042A, M0055A, M0056A, and M0057A (Fig. 6b, c; Fig. 7b). Crystals diameters range from 20-80 μm. They can either be found irregularly distributed between components, completely filling the pore space, and in primary grain porosity. Crystal sizes may be largely similar or increase from the margin towards the center of the filled pore space. Blocky spar was observed to form a second diagenetic phase after marine aragonite cement in holes M0042A, M0055A, M0056A, and M0057A (Fig. 6a, d). Scalenohedral (dogtooth) cement was identified in greatest abundance in holes M0042A and M0057A. Often lining open, unfilled porosity, and individual crystals getting as long as 80 μm (Fig. 6d, f). Syntaxial overgrowths on echinoderm fragments may be found occasionally (Fig. 7d), identified under crossed polars. Low-magnesium calcite cement with meniscus textures can be found in hole M0057A in depth 19-25 m downcore (Fig. 6e).

Mineralogy and geochemistry

On average, the pre-LGM samples consist of 32% aragonite, 9% high-magnesium calcite, and 59% low-magnesium calcite (Table 4). In holes M0042A and M0057A, aragonite percentages decrease and low-magnesium calcite percentages increase downcore. Quartz was identified in 17 samples, however, abundance does not usually exceed 2%. Dolomite was not observed. As expected, mineralogy data show correlations with abundances of certain common skeletal components, such as in corals and *Halimeda* with aragonite (Table 5). Likewise, all the correlations between the abundances of marine and meteoric cements exhibit statistically significant correlations with carbonate mineralogy (Table 5). Among the cores analyzed, the relative abundance of carbonate minerals is different, and three groups may be delineated. Samples from holes M0032A and M0033A as well as from the upper part of hole M0042A are composed of aragonite and high-magnesium calcite (>90%); the average abundance of low-magnesium calcite is <5%. Samples from hole M0057A are composed of 90% low-magnesium calcite and 10% aragonite on average. Only in the uppermost pre-LGM core sections (57 7 R1 81-130) high proportions of aragonite are observed. Samples in holes M0055A and M0056A display intermediate proportions in their carbonate mineralogy, and show mean abundances of 45% low-magnesium calcite, 37-55% aragonite, and 0-17% high-magnesium calcite.

Values of stable isotopes of oxygen ($\delta^{18}O$) in bulk samples range from -5.18‰ to +0.80‰ and carbon ($\delta^{13}C$) from -7.99‰ to +4.29‰ (Fig. 8; Table 4). Three data clouds can be delineated. Samples from holes M0032A and M0033A have high $\delta^{18}O$ (-1 to +1‰) and $\delta^{13}C$ (+1 to +4‰), whereas samples from holes M0057A and M0042A are characterized by lighter isotope ratios ($\delta^{18}O$: -4 to +2‰; $\delta^{13}C$: -8 to +2‰). Samples from the upper parts of these holes have intermediate isotope compositions plotting towards the upper right. The same is true for samples of holes M0055A and M0056A. $\delta^{18}O$ and $\delta^{13}C$ values show a strong

correlation (r=0.860, p<0.000), and significantly correlate positively with the abundances of marine cements and negatively with those of meteoric cements (Table 5). The downcore variability of $\delta^{18}O$ and $\delta^{13}C$ is shown on figure 2 and mostly exhibits no clear trends. Still, in holes M0042A and M0057A, heavier isotopes occur at the tops and lighter ones at the bases of analyzed intervals.

A cluster analysis of the diagenesis and geochemistry data including abundances of cements, secondary porosity, portions of aragonite, high-magnesium calcite, and low-magnesium calcite, and $\delta^{18}O$ and $\delta^{13}C$ values is used to classify the types of diagenesis present in these cores (Fig. 9). The analysis produces two distinct clusters and five subclusters. The upper cluster includes samples with marine diagenesis predominating as in holes M0032A, M0033A, and the upper parts of holes M0042A, M0056A, and M0057A. The lower cluster comprises samples that are characterized by predominating meteoric diagenesis as in holes M0042A, M0056A, and M0057A. The sub-clusters are largely produced based on variation in carbonate mineralogy (Fig. 10). The relatively low abundances of individual cement types as shown in Table 3 did not influence the clustering significantly.

DISCUSSION

Microfacies

Biogenic packstones and grainstones with diverse biota such as coralline algae, corals, *Halimeda*, benthic foraminifera, and mollusks have also been identified by previous studies analyzing the Great Barrier Reef Pleistocene in deposits younger than MIS 11 (International Consortium of Great Barrier Reef Drilling, 2001; Webster and Davies, 2003; Braithwaite *et al*., 2004) and recently in pre-LGM carbonate sequences off of the island of Tahiti (Iryu *et al*., 2010). Based on the observations made here and results from previous studies, the mixed skeletal- and coral- and coralgal-dominated microfacies are interpreted to have been deposited

in a reefal, high-energy environment at the shelf margin. This assumption is also supported by modern facies distribution patterns (Maxwell, 1968), and the elevations of the investigated core sections older than LGM at or close to relative sea level during their deposition (Fig. 11). The *Halimeda*-rich microfacies was either formed further inboard, in a back-reef setting, like *Halimeda*-rich surface sediments in the modern Great Barrier Reef (Maxwell, 1968). *Halimeda*-rich back-reef facies are also common in the Belize Barrier Reef in the western Atlantic Ocean (Purdy and Gischler, 2003). Alternatively, the *Halimeda* microfacies formed in a deeper shelf or fore reef-setting, as similar deposits from the Belize Barrier Reef (James and Ginsburg, 1979), the northern Great Barrier Reef (Marshall and Davies, 1988), the Nicaraguan Rise (Hine *et al*., 1988), or the Huon Gulf (Webster *et al*., 2004). Likewise, the occurrences of matrix-supported textures (mudstone-wackestone) were presumably also deposited in more protected and/or greater water depths, lower energy settings. Deposition was probably still adjacent to the shelf margin because the amount of siliciclastics in the mudstone-wackestone facies is negligible. Only towards mid and inner regions of the modern Queensland shelf, the amounts of terrigenous clay and silt in surface sediments increase considerably (Maxwell, 1968; Hopley, 2007). Interestingly, coarse siliciclastics such as quartz grains increase from the inner to the outer shelf and towards the offshelf realm (Francis *et al*., 2007). This observation appears to oppose the widely held concept of reciprocal shedding of carbonates and siliciclastics during highstands and lowstands of sea level, respectively. The mechanisms that transport siliciclastics across the Queensland shelf, however, are only poorly constrained.

The limited pre-LGM microbialite development probably occurred in reef cavities, just like the postglacial examples of Tahiti (Seard *et al*., 2011). The latter exhibit both laminated and thrombolitic textures (Westphal *et al*., 2010). Like their post-LGM counterparts, the pre-LGM microbialites studied here are made of abundant high-magnesium

calcite (46%). The existence of considerable amounts of low-magnesium calcite and blocky cement indicates diagenetic alteration in the meteoric realm. The laminar fabric that predominates here could be the result of repeated growth of microbial mats. Macroscopically, the pre-LGM microbialites resemble zebra limestone (Fischer, 1964), which is a typical component in Phanerozoic mud-mounds (Monty, 1995). The rare thrombolitic textures resemble the spongiform texture that is seen also in carbonate mud-mounds (Pratt, 1982). The low numbers of microbialites in the pre-LGM sections are most likely a consequence of the formation during falling sea-level trends (Fig. 11). For comparison, abundant microbialite formation off of Tahiti is preferentially observed during rapid sea-level rise, like during the post-LGM, that leads to relatively open frameworks that can potentially be colonized by microbes (Saerd *et al*., 2011). Microbialite appears to be less commmon in pre-LGM deposits around Tahiti (Iryu *et al*., 2010).

The caliche features observed such as lamination, brown-red staining, motttled and clotted textures, and rhizoliths are clear indications of subaerial exposure (James, 1972; Harrison and Steinen, 1978). Laminated portions of caliche may be readily distinguished from microbialite based on the lack of zebra limestone-type textures in the former.

Diagenesis

Features of marine phreatic features diagenesis include micrite envelopes, acicular (needle), botryoidal, microcrystalline, and peloidal cements (*e.g.*, Longmann, 1980; Harris et al., 1985; and references therein). Marine cements are most common in coral packstone and grainstone and in *Halimeda* grainstone with abundant primary porosity. Likewise, meteoric cements are most abundant in grain-supported textures.

Reid and Macintyre (2000) have shown how endolithic activity of cyanobacteria (*Solentia* sp.) with subsequent precipitation of aragonite in bored cavities can lead to

micritization of grain margins and eventually even entire grains. Our study has shown that endolithic activity did not only occur relatively early but also after the formation of the first generation of marine cementation because aragonite cement exhibits micrite envelopes as well. The reasons for this observation are not entirley clear, however, growth of marine cement at shelf margins may be a very rapid process (Grammer *et al*., 1993, 1999), i.e., only little time could be involved in the formation of the two generations of micrite envelopes. Isopachous crusts of needle or acicular cements have been identified to be common in the early marine phreatic realm (Longman, 1980; Macintyre and Marshall, 1988). Like the acicular type, botryoidal aragonite cement forms typically in the marine phreatic realm and was first described from from deeper fore reef deposits of the Belize Barrier Reef (Ginsburg and James, 1976). The formation of peloidal cement has been attributed to both inorganic processes (Macintyre and Marshall, 1988) and microbial activity (Chafetz, 1986). In this study, it was observed that peloidal texture may be produced by neomorphism of coralline algal fragments (Fig. 7f). As explained and discussed by Friedman (1985) and Reid et al. (1990), it is often difficult to determine whether micrcrystalline cement is indeed a marine cement or fine-grained detrital marine sediment.

In most of the pre-LGM facies, diagenetic alteration such as dissolution and blocky cement growth (*e.g.*, Land, 1970; Longmann, 1980; Harris et al., 1985; and references therein) can be seen first in hand specimens and in detail in thin-section. Grain dissolution and neomorphism are common diagenetic features both in the meteoric (*e.g.*, Gvirtzman and Friedmann, 1977; Quinn, 1991; Strasser *et al*., 1992) and the shallow marine-burial (Dix and Mullins, 1988; Melim *et al*., 1995) diagenetic realms of carbonate platforms and reefs. Like dissolution and neomorphism, the formation of blocky cement is characteristic of the meteoric and burial realms (*e.g.*, Longmann, 1980; Harris *et al*., 1985; Melim *et al*., 1995). Dogtooth or bladed low-magnesium calcite cement has been interpreted as a meteoric cement (Quinn,

1991). As it occurs in close proximity with blocky spar and in many cases postdates blocky cement, it could be either a meteoric-phreatic or an early marine-burial type. Syntaxial cement has been decribed first by Evamy and Shearman (1965), and is interpreted as characteristic of the meteoric-phreatic realm (*e.g*., Longmann, 1980). Meniscus textures as seen from 19-25 m depth in hole M0057A are indicative of the meteoric-vadose diagenetic zone (Land, 1970; Bricker, 1971; Longmann, 1980; Harris *et al*., 1985).

Recent subsurface studies of late Pleistocene reefs at Ribbon Reef 5 (Braithwaite and Montaggioni, 2009), the holes of which were excluded from our study, and at Mururoa (Braithwaite and Camoin, 2011) exhibit many similar marine and meteoric cement types and neomorphism and dissolution patterns. The variety and abundance of cements appears to be higher in Mururoa though. Diagenetic patterns in pre-LGM deposits of Tahiti, however, differ from our findings in that marine-phreatic, equant low-magnesium calcite cements are rather rare (Woo *et al*., 2010).

Mineralogical analyses of bulk samples, including cluster analyses, largely confirm the results of observations made in thin-section. Samples that do not show neomorphism and marine-phreatic diagenesis (M0032A, M0033A) are dominated by aragonite and high-magnesium calcite mineralogies. Core section that exhibit meteoric diagenesis are dominated by low-magnesium calcite (lower part M0042A, M0057). Samples from holes M0055A, M0056A, and upper part M0042A are intermediate.

Isotope analyses of bulk samples show similar patterns and allow to largely exclude the possible influence of marine-burial diagenesis, which may produce similar cement morphologies and alteration as meteoric diagenesis (Freeman-Lynde *et al*., 1986; Dix and Mullins, 1988; Melim *et al*., 1995). Samples from holes M0032A and M0033A have heavier stable oxygen and carbon isotopes (Fig. 8) indicating a marine signal, whereas samples from holes M0057A and M0042A (lower part) largely have lighter isotope compositions clearly

suggesting meteoric influence (*e.g.*, Allan and Matthews, 1977, 1982; Melim *et al*., 1995). Samples from the upper parts of these holes plot towards the upper right of the isotope plot (Fig. 8) as a consequence of both marine and meteoric diagenesis. The same is true for samples of holes M0055A and M0056A, which plot inbetween the typical marine and meteoric fields. Comparable studies in the subsurface of Ribbon Reef 5 (Braithwaite and Montaggioni, 2009, their Fig. 10) and in Mururoa (Braithwaite and Camoin, 2011, their Fig. 7) have produced strikingly similar isotope distribution patterns of late Pleistocene reefal deposits and cements.

Multiple generations of cement from different diagenetic environments are not observed in the investigated samples. For example, samples in hole M0042A with a maximum age of about 169 kyrs BP should have experienced two phases each of marine and meteoric diagenesis (Fig. 11), and samples in hole M0057A possibly even more during successive Pleistocene sea-level variations. However, these are not recorded in the diagenetic signatures. For reasons not entirely clear, only one diagenetic change from marine-phreatic to meteoric-phreatic is observed. Vollbrecht (1990) made similar observations in Pleistocene platform carbonates of Bermuda and concluded that the diagenetic record was incomplete. Only a few Pleistocene highstand shorelines near the margin of the Bermuda platform recorded multiple diagenetic changes (Vollbrecht and Meischner, 1996). These authors concluded that diagenetic (cement) recording of repeated sea-level change is rare in reefs, that prevasive geochemical signatures rather than delicate cement sequences would record pore water change more readily, and that strong meteoric diagenesis commonly destroys earlier cement fabrics. As already shown by Steinen and Matthews (1973) in Pleistocene reefal deposits on the island of Barbados, the meteoric-phreatic zone is much more diagenetically active as compared to both the meteoric-vadose and marine-phreatic zones. The same appears to be true for the Great Barrier Reef samples. Possibly, the abundant blocky spar in samples

from cores M0042A and M0057A represents two or more generations of meteoric cement, while only the first marine generation of cement is preserved in the youngest holes. Another explanation for the lack of multiple cement generations could be the control of substrate mineralogy on overgrowth mineralogy (Burton, 1993). This author has shown in laboratory experiments that aragonite cements preferentially grow on aragonite substrates and calcite cements on calcite substrates. However, as natural examples of multiple diagenetic records exists, although usually in an incomplete manner (*e.g.*, Vollbrecht and Meischner, 1996; Sherman *et al*., 1999), additional factors are apparently able to neutralize the substrate control. Braithwaite and Montaggioni (2009) found in their Ribbon Reef 5-study that cements were arranged discontinuously in the Pleistocene sequences and also noted a limited distribution of multiple cement generations. Likewise, Braithwaite and Camoin (2011) realized that only some sea-level cycles are reflected in diagenetic features, despite the fact that a large variety of both marine and meteoric cements including cement sequences are described in their Mururoa study. These authors argued that the "temporally varying positions of the vadose-phreatic and meteoric-marine groundwater boundaries conspire against the generation of any uniform sequence" of cements.

The degree of marine diagenesis shows no statistically significant correlation with elevation, however, abundance of meteoric diagenesis is correlated negatively with depth below sea level (Table 5). Notably, the only horizon exhibiting meteoric-vadose diagenesis (hole M0057A, 19-25 m) was found in the shallowest location. Samples with higher elevation were potentially exposed in the meteoric realm for a longer time span during late Pleistocene sea-level change as seen in the depth distribution of stable isotope values that may be used as a proxy of diagenesis (Fig. 12a). At the same time, however, greater depth below the sea floor appears to have favored meteoric-phreatic diagenesis as negative stable isotope values are found deeper in the sediment (Fig. 12b). This observation would by trend oppose the model of

Melim (1996) that predicts shallower meteoric water lenses during minor sea-level falls being more active than deeper freshwater lenses that form during major falls. During the latter scenario, groundwater potentially gets saturated with regard to calcium carbonate before reaching a deep lens, and the lens is further away from soil organic matter the degradation of which will be conducise for meteoric diagenesis. However, in order to apply models like this to our study, additional age data are needed in order to constrain the relationships between sea level, diagenetic patterns, and the frequently changing groundwater levels during the late Pleistocene.

CONCLUSIONS

Based on our analyses of samples from the pre-LGM deposits we draw the following main conclusions:

- Pre-LGM microfacies in samples from the Great Barrier Reef (IODP 325) are largely mixed skeletal grainstones and packstones. Eleven microfacies were delineated, with matrix-supported textures being less common. The majority of facies formed in a high energy, marginal platform environment.
- Unlike in the postglacial sections that exhibit abundant microbial activity, microbialite is uncommon in pre-LGM samples, most likely as a consequence of more limited formation during falling sea-level trends. Apparently, rapid rising sea level produces more abundant cavities in open reef framework that can potentially be colonized by microbes.
- Diagenesis shows marine-phreatic, meteoric-phreatic, and meteoric-vadose patterns. The diagenetic record is not complete, and only one pore water change from marine to meteoric was observed. Apparently, the meteoric-phreatic realm is diagenetically most active.

ACKNOWLEDGEMENTS

This research used samples and/or data provided by the Integrated Ocean Drilling Program (IODP). Funding for this research was provided by the Deutsche Forschungsgemeinschaft (to E. Gischler) and by the Australian Research Council ARC, discovery grant DP1094001 (to J. Webster). We thank Anja Isaack, Friederike Adomat, and Matthias Rehbein for sample preparations for X-ray diffractometry and isotope geochemistry. Rainer Petschick ran the diffractometer. Thin-sections were made by Maria Bladt and Eckehard Gottwald. David Storz assisted during statistical analyses.

REFERENCES

Abbey, E., Webster, J.M. and **Beman, R.J. (2011)** Geomorphology of submerged reefs on the shelf edge of the Great Barrier Reef: The influence of oscillating sea-levels. *Mar. Geol*., **288**, 61-78.

Allen, J.R. and **Matthews, R.K.** (1977) Carbon and oxygen isotopes as diagenetic and stratigraphic tools: surface and subsurface data, Barbados, West Indies. *Geology*, **5**, 16-20.

Allen, J.R. and **Matthews, R.K.** (1982) Isotope signatures associated with early meteoric diagenesis. *Sedimentology*, **29**, 797-817.

Bard, E., Hamelin, B, Arnold, M., Montaggioni, L, Cabioch, G, Faure, G. and **Rougerie, F.** (1996) Deglacial sea-level record from Tahiti corals and the timing of global meltwater discharge. *Nature*, **382**, 241-244.

Bard, E., Hamelin, B. and **Delanghe-Sabatier, D.** (2010) Deglacial meltwater pulse 1B and Younger Dryas sea levels revisited with boreholes at Tahiti. *Science*, **327**, 1235-1237.

Braithwaite, C.J.R. and Camoin, G.F. (2011) Diagenesis and sea-level change: lessons from Moruroa, French Polynesia. *Sedimentology*, **58**, 259-284.

Braithwaite, C.J.R., Dalmasso, H., Gilmore, M.A., Harkness, D.D., Henderson, G.M., Kay, R.L.F., Kroon, D., Montaggioni, L.F. and **Wilson, P.A.** (2004) The Great Barrier Reef: the chronological record from a new borehole. *J. Sed. Res*., **74**, 298-310.

Braithwaite, C.J.R. and **Montaggioni, L.F.** (2009) The Great Barrier Reef: a 700 000 year diagenetic history. *Sedimentology*, **56**, 1591-1622.

Bricker, O.P. (Ed) (1971) Carbonate cements. *Johns Hopkins Univ. Stud. Geol*., **19**, 376 p.

Burton, E.A. (1993) Controls on marine carbonate cement mineralogy: review and assessment. *Chem. Geol*., **105**, 163-179.

Cabioch, G., Montaggioni, L., Thouveny, N., Frank, N., Sato, T., Chazottes, V., Dalamasso, H., Rayri, C., Pichon, M. and **Demah, A.M.** (2008) The chronology and structure of the western New Caledonian barrier reef tracts. *Palaeogeogr. Palaeoclimatol. Palaeoecol*., **268**, 91-105.

Camoin, G.F., Ebren, P., Eisenhauer, A., Bard, E. and **Faure, G.** (2001) A 300 000-yr coral reef record of sea level changes, Mururoa Atoll (Tuamotu archipelago, French Polynesia). *Palaeogeogr. Palaeoclimatol. Palaeoecol*., **175**, 325-341.

Camoin, G.F., Iryu, Y., McInroy, D.B., and **Expedition 310 Scientists** (2007) *Proceedings IODP, 310*, Integrated Ocean Drilling Program Management International, Inc., Washington DC doi:10.2204/iodp.proc.310.2007

Chafetz, H.S. (1986) Marine peloids: a product of bacterially induced lithification of microbial crusts. *J. Sed. Petrol*., **56**, 812-817.

Chappell, J. (1974) Geology of coral terraces, Huon Peninsula, New Guinea: a study of Quaternary tectonic movements and sea-level changes. *Geol. Soc. Amer. Bull*., **85**, 553-570.

Chappell, J. and **Polach, H.** (1991) Post-glacial sea-level rise from a coral record at Huon Peninsula, Papua New Guinea. *Nature*, **349**, 147-149.

Dix, G.E. and **Mullins, H.T.** (1988) Rapid burial diagenesis of deep-water carbonates: Exuma Sound, Bahamas. *Geology*, **16**, 680-683.

Droxler, A., Alley, R.B., Howard, W.R., Poore, R.Z. and **Burckle, L.H.** (2003) Unique and exceptionally long interglacial isotope stage 11: window into earth warm future climate. In: *Earth`s Climate and Orbital Eccentricity. The Marine Isotope Stage 11 Question* (Eds Droxler, A.W., Poore, R.Z. and Burckle, L.H.), *Geophys. Monogr*., **137**, 1-14.

Dullo, W.C. (1987) The role of microarchitecture and microstructure in the preservation of reef corals: a case study from the Pleistocene of Barbados. *Facies*, **16**, 11-22.

Dullo, W.C. (1990) Facies, fossil record, and age of Pleistocene reefs from the Red Sea (Saudi Arabia). *Facies*, **22**, 1-46.

Edwards, R.L., Chen, J.H. and **Wasserburg, G.J.** (1986) ^{238}U-^{234}U-^{230}Th-^{232}Th systematics and the precise measurement of time over the past 500,000 years. *Earth Planet. Sci. Lett*., **81**, 175–192.

Evamy, B.D. and **Shearman, D.J.** (1965) The development of overgrowths from echinoderm fragments. *Sedimentology*, **5**, 211-233.

Fairbanks, R.G. (1989) A 17,000 year glacio-eustatic sea level record: influence of glacial melting rates on the Younger Dryas event and deep ocean circulation. *Nature*, **342**, 637-642.

Felis, T., Lohmann, G., Kuhnert, H., Lorenz, S.J., Scholz, D., Pätzold, J., Al-Rousan, S. and **Al-Moghrabi, S.** (2004) Increased seasonality in Middle East temperatures during the last interglacial period. *Nature*, **429**, 164-168.

Fischer, A.G. (1964) The Lofer cyclothems of the Alpine Triassic. *Kansas Geol. Surv. Bull*., **169**, 107-149.

Francis, J.M., Dunbar, G.B., Dickens, G.R., Sutherland, I.A. and **Droxler, A.W.** (2007) Siliciclastic sediment across the north Queensland margin (Australia): a Holocene

prespective on reciprocal versus coeval deposition in tropical mixed siliciclastic-carbonate systems. *J. Sed. Res*., **77**, 572-586.

Freeman-Lynde, R.P., Whitley, K.F. and **Lohmann, K.C.** (1986) Deep-marine origin of equant spar cements in Bahama escarpment limestones. *J. Sed Petrol*., **56**, 799-811.

Friedman, G.M. (1959) Identification of carbonate minerals by staining methods. *J. Sed. Petrol*., **29**, 87-97.

Friedman, G.M. (1985) The problem of submarine cement in classifying reefrock: an experience in frustration. In: Carbonate Cements (Eds Schneidermann, N. and Harris, P.M.), *Soc. Econ. Pal. Min. Spec. Publ*., **36**, 117-121.

Ginsburg, R.N. and **James, N.P.** (1976) Submarine botryoidal aragonite in Holocene reef limestones, Belize. *Geology*, **4**, 431-436.

Gischler, E., Hudson, J.H. and **Storz, D.** (2009) Growth of Pleistocene massive corals in south Florida: low skeletal extension rates and possible ENSO, decadal, and multi-decadal cyclicities. *Coral Reefs*, **28**, 823-830.

Gischler, E. Ginsburg, R.N., Herrle, J.O. and **Prasad, S.** (2010) Mixed carbonates and siliciclastics in the Quaternary of southern Belize: Pleistocene turning points in reef development controlled by sea-level change. *Sedimentology*, **47**, 1049-1068.

Grammer, G.M., Crescini, C.M., McNeill, D.F. and **Taylor, L.H. (1999)** Quantifying rates of syndepositional marine cementation in deeper platform environments - new insight into a fundamental process. *J. Sed. Res*., **69**, 202-207.

Grammer, G.M., Ginsburg, R.N., Swart, P.K., McNeill, D.F., Jull, A.J. and **Prezbindowsky, D.R.** (1993) Rapid growth rates of syndepositional marine aragonite cements in steep marginal slope deposits, Bahamas and Belize. *J. Sed. Petrol*., **63**, 983-989.

Gvirtzman G. and **Friedman G.M.** (1977) Sequence of progressive diagenesis in coral reefs. In: Reefs and related carbonates - ecology and sedimentology (Eds Frost, S.H., Weiss, M.P. and Saunders, J.B.), *Amer. Assoc. Petrol. Geol. Stud. Geol*., **4**, 357-380.

Harris, P.M., Kendall, C.S.C. and **Lerche, I.** (1985): Carbonate cementation - a brief review. In: Carbonate Cements (Eds Schneidermann, N. and Harris, P.M.), *Soc. Econ. Pal. Min. Spec. Publ*., **36**, 79-95.

Harrison, R.S. and **Steinen, R.P.** (1978) Subaerial crusts, caliche profiles and breccia horizons; comparison of some Holocene and Mississippian exposure surfaces, Barbados and Kentucky. *Geol. Soc. Amer. Bull*., **89**, 385-396.

Hine, A.C., Hallock, P., Harris, M.W., Mullins, H.T., Belknap, D.F. and **Jaap, W.C.** (1988) *Halimeda* bioherms along an open seaway: Miskito Channel, Nicaraguan Rise, SW Caribbean Sea. in: *Halimeda* (Eds Roberts, H.H. and Macintyre, I.G.), *Coral Reefs*, **6**, 173-178.

Hopley, D., Smithers, S.G. and **Parnell, K.E.** (2007) *The geomorphology of the Great Barrier Reef. Development, diversity, and change*. Univ. Press, Cambridge, 532 p.

International Consortium Great Barrier Reef Drilling (2001) New constraints on the origin of the Australian Great Barrier Reef: results from an international project. *Geology*, **29**, 483-486.

Iryu, Y., Yasunari, T., Fujita, K., Camoin, G., Cabioch, G., Matszda, H., Sato, T., Sugihara, K., Webster, J.M. and **Westphal, H.** (2010) Sealevel history recorded in the Pleistocene carbonate sequence in IODP hole 310-M0005D, off Tahiti. *Island Arc*, **19**, 690-706.

Jackson, J.B.C. (1992) Pleistocene perspectives on coral reef community structure. *Amer. Zool*., **32**, 719-731.

James, N.P. (1972) Holocene and Pleistocene calcareous crust (caliche) profiles: criteria for subaerial exposure. *J. Sed. Petrol*., **42**, 817-836.

James, N.P. and **Ginsburg, R.N.** (1979) The seaward margin of Belize barrier and atoll reefs. *Int. Assoc. Sedimentol. Spec. Publ*., **3**, 191 pp.

Kievman, C.M. (1998) Match between late Pleistocene Great Bahama Bank and deep-sea oxygen isotope records of sea level. *Geology*, **26**, 635-638.

Land, L.S. (1970) Phreatic versus vadose meteoric diagenesis of limestones: evidence from a fossil water table. *Sedimentology*, **14**, 175-185.

Lisiecki, L.E. and **Raymo**, M.E. (2005) A Pliocene-Pleistocene stack of 57 globally distributed benthic $d^{18}O$ records. *Paleoceanography*, **20**, PA1003, doi: 10.1029 / 2004 PA 001071.

Longmann, M.W. (1980) Carbonate diagenetic textures from near-surface diagenetic environments. *Amer. Assoc. Petrol. Geol. Bull.*, **64**, 461-487.

Macintyre, I.G. and **Marshall, J.F.** (1988) Submarine lithification in coral reefs: some facts and misconceptions. *Proc. 6th Int. Coral Reef Symp*., **1**, 263-272.

Marshall, J.F. and **Davies, P.J.** (1984) Last interglacial reef growth beneath modern reefs in the southern Great Barrier Reef. *Nature*, **307**, 44-46.

Marshall, J.F. and **Davies, P.J.** (1988) *Halimeda* bioherms of the northern Great Barrier Reef. In: *Halimeda* (Eds Roberts, H.H. and Macintyre, I.G.), *Coral Reefs*, **6**, 139-148.

Maxwell, W.G.H. (1968) *Atlas of the Great Barrier Reef*. 258 p., Elsevier, New York.

Mazzullo, S.J. (2006) Late Pliocene to Holocene platform evolution in northern Belize, and comparison with coeval deposits in southern Belize and the Bahamas. *Sedimentology*, **53**, 1015-1047.

Melim, L.A. (1996) Limitations on lowstand meteoric diagenesis in the Pliocene-Pleistocene of Florida and Great Bahama Bank: implications for eustatic sea-level models. *Geology*, **24**, 893-896.

Melim, L.A., Swart, P.K. and **Maliva, R.G.** (1995) Meteoric-like fabrics forming in marine waters: implications for the use of petrography to identify diagenetic environments. *Geology*, **23**, 755-758.

Mesolella, K.J. (1967) Zonation of uplifted Pleistocene coral reefs on Barbados, West Indies. *Science*, **156**, 638-640.

Miller, K.G., Kominz, M.A., Browning, J.V., Wright, J.D., Mountain, G.S., Katz, M.E., Sugarman, P.J., Cramer, B.S., Christie-Blick, N. and **Pekar, S.F.** (2005) The Phanerozoic record of global sea-level change. *Science*, **310**, 1293-1298.

Milliman, J.D. (1974) *Marine Carbonates*. 375 p., Springer, New York.

Montaggioni, L.F., Cabioch, G., Thouveny, N., Frank, N., Sato, T. and **Semah, A.M.** (2011) Revisiting the Quaternary development history of the western New Caledonian shelf system: from ramp to barrier reef. *Mar. Geol*., **280**, 57-75.

Monty, C.L.V. (1995) The rise of carbonate mud-mounds: an introductory actualistic approach. In Carbonate mud-mounds. Their origin and evolution (Eds Monty, C.L.V., Bosence, D.W.J., Bridges, P.H. and Pratt, B.R.), *Int. Assoc. Sedimentol. Spec. Publ*., **23**, 11-49.

Multer, H.G., Gischler, E., Lundberg, J., Simmons, K. and **Shinn, E.A.** (2002) The Key Largo Limestone revisited: Pleistocene shelf edge facies, Florida Keys, USA. *Facies*, **46**, 229-272.

Pandolfi, J. (1996) Limited membership in Pleistocene reef coral assemblages from the Huon Peninsula, Papua New Guinea: constancy during global change. *Paleobiol.*, **22**, 152-176.

Pratt, B.R. (1982) Stromatolitic framework of carbonate mud-mounds. *J. Sed. Petrol*., **52**, 1203-1227.

Purdy, E.G. and **Gischler, E.** (2003) The Belize margin revisited: 1. Holocene marine facies. *Int. J. Earth Sci*., **92**, 532-551.

Purdy, E.G. and **Winterer, E.L.** (2006) Contradicting barrier reef relationships for Darwin's evolution of reef types. *Int. J. Earth Sci*., **95**, 143-167.

Quinn, T.M. (1991) Meteoric diagenesis of Plio-Pleistocene limestones at Enewetak Atoll. *J. Sed. Petrol*., **61**, 681-703.

Reid, R.P. and **Macintyre, I.G.** (2000) Microboring versus recrystallization: further insight into the micritization process. *J. Sed. Res*., **70**, 24-28.

Reid, R.P., Macintyre, I.G. and **James, N.P.** (1990) Internal precipitation of microcrystalline carbonate: a fundamental problem for sedimentologists. *Sed. Geol*., **68**, 163-170.

Schroeder, J.H. and **Purser, B.H.** (eds) (1986) *Reef diagenesis*. Springer, Berlin, 455 p.

Seard, C., Camoin, G., Yokoyama, Y., Matsuzaki, H., Duranda, N., Bard, E., Sepulcrea, S. and **Deschamps, P.** (2011) Microbialite development patterns in the last deglacial reefs from Tahiti (French Polynesia; IODP Expedition #310): Implications on reef framework architecture. *Mar. Geol*., **279**, 63-86.

Sherman, C.E., Fletcher, C.H. and **Rubin, K.H.** (1999) Marine and meteoric diagenesis of Pleistocene carbonates from a nearshore submarine terrace, Oahu, Hawaii. *J. Sed. Res*., **69**, 1083-1097.

Spötl, C. and **Vennemann, T.** (2003) Continuous-flow isotope ratio mass spectrometric analysis of carbonate minerals. *Rapid Comm. Mass Spect.*, **17**, 1004-1006.

Stanley, S.M. (1966) Paleoecology and diagenesis of Key Largo Limestone, Florida. *Amer. Assoc. Petrol. Geol. Bull*., **50**, 1927-1947.

Steinen, R.P. and **Matthews, R.K.** (1973) Phreatic vs. vadose diagenesis: stratigraphy and mineralogy of a cored borehole on Barbados, W.I. *J. Sed. Petrol.*, **43**, 1012-1020.

Strasser, A., Strohmenger, C., Davaud, E. and **Bach, A.** (1992) Sequential evolution and diagenesis of Pleistocene coral reefs (south Sinai, Egypt). *Sed. Geol.*, **78**, 59-79.

Tudhope, A.W., Chilcott, C.P., McCulloch, M.T., Cook, E.R., Chappell, J., Ellam, R.M., Lea, D.W., Lough, J.M. and **Shimmield, G.B.** (2001) Variability in the El Niño-southern oscillation through a glacial-interglacial cycle. *Science*, **291**, 1511-1517.

van der Plaas, L. and **Tobi, A.C.** (1965) A chart for judging the reliability of point-counting results. *Amer. J. Sci.*, **263**, 87-90.

Vollbrecht, R. (1990) Marine and meteoric diagenesis of submarine Pleistocene carbonates from the Bermuda carbonate platform. *Carb. Evap.*, **5**, 13-95.

Vollbrecht, R. and **Meischner D.** (1996) Diagenesis in coastal carbonates related to Pleistocene sea level, Bermuda Platform. *J. Sed. Res.*, **66**, 243-258.

Webster, J.M. and **Davies, P.J.** (2003) Coral variation in two deep drill cores: significance for the Pleistocene development of the Great Barrier Reef. *Sed. Geol.*, **159**, 61-80.

Webster, J.M., Wallace, L., Silver, E., Potts, D., Braga, J.C., Renema, W., Riker.Coleman, K. and **Gallup, C.** (2004) Coralgal composition of drowned carbonate platforms in the Huon Gulf, Papua New Guinea; implications for lowstand reef development and drowning. *Mar. Geol.*, **204**, 59-89.

Webster, J.M., Yokoyama, Y, Cotterill, C and **Expedition 325 Scientists** (2011) Great Barrier Reef environmental changes: the last deglacial sea level rise in the South Pacific: offshore drilling northeast Australia. *Proc. Integr. Ocean Drill. Prog..*, **325**, doi:10.2204/iodp.proc.325.2011

Westphal, H., Heindel, K., Brandano, M. and **Peckmann, J.** (2010) Genesis of microbialites as contemporaneous framework components of deglacial reefs, Tahiti (IODP 310). *Facies*, **56**, 337-352.

Woo, K.S., Yoon, K.H., Lee, Y.J., Yamada, T., Asami, R. and **Iryu, Y.** (2010) Carbonate diagenesis of the late Pleistocene limestone of the Faaa M0020A core: IODP Expedition 310, Tahiti Sea Level Change. *Geosc. J.*, **14**, 225-234.

Yokoyama, Y. and **Esat, T.M.** (2011) Global climate and sea level. Enduring variability and rapid fluctuations over the past 150,000 years. *Oceanogr.*, **24**, 54-69.

Yokoyama, Y., Purcell, A., Marshall, J.F. and **Lambeck, K.** (2006) Sea-level during the early deglaciation period in the Great Barrier Reef, Australia. *Global Planet. Change*, **53**, 147-153.

Yokoyama, Y., Webster, J.M., Cotterill, C., Braga, J.C., Jovane, L., Mills, H., Morgan, S., Suzuki, A. and **IODP Expedition 325 Scientists** (2011) IODP Expedition 325: Great Barrier Reef reveals past se-level, climate and environmnetal change since the last ice age. *Sci. Drill.*, **12**, 32-45.

FIGURE CAPTIONS

Fig. 1. Drill locations including investigated holes of IODP Expedition 325 along the Great Barrier Reef (reefs and shoals in black). Reefs and shoals on Queensland Plateau east of Cairns (Coral Sea) are not shown. RIB = Ribbon Reef; NOG = Noggin Pass; HYD = Hydrographer's Passage. Map modified from Purdy and Winterer (2006, their Fig. 13).

Fig. 2. (a) Core logs of holes M0032A, M0033A, and M0042A. (b) Core logs of holes M0055A, M0056A, and M0057A. Lithologies are taken from Webster et al. (2011). Microfacies delineated during this study are shown using abbreviations in the text. To the right of the columns, diagenesis from cluster analysis (Fig. 9), isotope geochemistry (open circles for $\delta^{18}O$ and closed circles for $\delta^{13}C$), mineralogy (open squares), and chronology data are plotted. Ara/Cal = ratio of aragonite and calcite abundances. Stable isotope data also shown on figure 7.

Fig. 3. Photographs of older Pleistocene hand specimens. (a) Coralline algal grainstone with rhizolith (brown). Hole 42, core 25, 54-59 cm; ca. 88 m below sea level (SL). (b) *Halimeda* grainstone. Hole 55, core 7, 11-17 cm; ca. 107 m below SL. (c) *Halimeda* grainstone with coral fragment and thin caliche (brown). Hole 57, core 7, 38-51 cm; ca. 61 m below SL. (d) Caliche (brown) in coral-algal packstone. Hole 57, core 13; ca. 115 m below SL. (e) Diagenetically altered faviid(?) coral. Hole 55, core 6, 66-77 cm; ca. 115 m below SL. (f) Coral grainstone with clear signs of meteoric alteration. Hole 56, core 2, 81-98 cm; ca. 86 m below SL. (g) Mixed skeletal packstone with dissolution cavities that are partially filled by fine-grained internal sediment. Hole 57, core 14-R2, 48-70 cm; ca. 77 m below SL. (h)

Altered microbialite, reminescent of zebra limestone. Hole 57, core 7, 52-59 cm; ca. 100 m below SL.

Fig. 4. Tree diagram of a cluster analysis (Ward's method) based on abundance data of constituent particles produces eleven microfacies. Ward's algorhithm was used because it exhibited the most meaningful results.

Fig. 5. Thin-section micrographs showing microfacies and marine and meteoric diagenesis. (a) Mixed skeletal packstone. Gastropod shell lined on inner side with aragonite needle cement; peloidal cement fills most of the inner shell. Hole 33, core 16, 59-65 cm. (b) Coralline algal grainstone. Partly dissolved and neomorphosed coralline algal fragment. Blocky cement lines dissolved cavity. Hole 42, core 23, 10-13 cm. (c) Coralline algal packstone with mollusk shells, *Halimeda*, and coral fragments. Note dissolution of gastropod shells (mouldic porosity). Hole 42, core 23, 10-13 cm. (d) Microbialite that shows irregular lamination. Note abundant small cavities and incorporation of small skeletal fragments. Hole 56, core 7, 52-59 cm. (e) Caliche developed within mixed skeletal packstone, with mottled texture and brecciation. Hole 57, core 14, 81-86 cm. (f) Caliche with possible diagenetic geopetals. Hole 56, core 9, 7-18 cm.

Fig. 6. Thin-section micrographs exhibiting microfacies and marine and meteoric diagenesis. (a) *Halimeda* grainstone. *Halimeda* and coral fragments with marine acicular cement and meteoric blocky cement. Note that micrite envelopes occur on grains boundaries and on marine cements. Hole 42, core 11, 27-33 cm. (b) *Halimeda* grainstone. Neomorphosed coral with interparticle porosity filled by microcrystalline, peloidal, and blocky cements. Hole 42, core 28, 33-37 cm. (c) *Halimeda* grainstone. Neomorphosed and partly dissolved *Halimeda*

fragments and blocky and dogtooth cements in packstone. Hole 56, core 14, 38-41 cm. (d) *Halimeda* grainstone. *Halimeda* and other biogenic fragments with acicular (marine) and dogtooth (meteoric) cements. Note micrite envelopes on marine cement fringe. Core 57, barrel 7, 105-108 cm. (e) *Halimeda* grainstone. *Halimeda* fragments with blocky cement and meniscus texture (meteoric vadose environment) in grainstone. Hole 57, core 8, 30-35 cm. (f) Mixed skeletal grainstone. Biogenic fragments in boundstone that shows strong signs of dissolution. Fragment in lower left corner is coralline alga. Pores lined with blocky and dogtooth (scalenohedral) cements. Hole 57, core 13, 10-15 cm.

Fig. 7. Thin-section micrographs exhibiting microfacies and marine and meteoric diagenesis. (a) Coralline algal grainstone. Encrusting foraminifer (*Carpenteria* sp.) with blocky cement in intraskeletal porosity. Hole 42, core 25, 54-59 cm. (b) Coral-algal packstone. Benthic foraminifer with micrite envelope and cemented by blocky spar. Hole 42, core 11, 33-37 cm. (c) Coral grainstone. Botryoidal (center) and needle (lower left) cement in primary porosity of coral. Hole 32, core 13, 14-18 cm. (d) Mixed skeletal grainstone. Syntaxial cement around echinoid spines. Hole 55, core 7, 18-25 cm. (e) Mixed skeletal packstone. Mollusk shell that is neomorphosed to blocky spar. Hole 42, core 25, 42-28 cm. (f) Coralline algal grainstone. Algal fragment that towards the top is altered to peloidal texture. Hole 42, core 25, 54-59 cm.

Fig. 8. Oxygen and carbon isotope values of older Pleistocene (pre-LGM) samples. Typical marine samples plot in the slightly positive area of the graph; samples under the influence of meteoric diagenesis plot in the negative quadrant of the graph.

Fig. 9. Tree diagram of a cluster analysis (Ward's method) based on diagenesis, mineralogy, and stable isotope geochemistry data. Ward's algorhithm was used because it produced the most meaningful results.

Fig. 10. Ternary diagram of carbonate mineralogy with samples highlighted according to membership in diagenetic sub-clusters in Figure 9. ARA = aragonite; LMC = low-magnesium calcite; HMC = high-magnesium calcite.

Fig. 11. U/Th-series ages of from older Pleistocene (pre-LGM) samples plotted on late Pleistocene sea-level data from the Huon Peninsula, New Guinea, and the Bonparte Gulf, Australia (Yokoyama and Esat, 2011). The isostatic influence on local deglacial sea level is estimated to be in the order of max. 20-25 m (Yokoyama *et al*., 2006). Sea-level data older than 140 kyrs BP is not plotted.

Fig. 12. (a) Cross plot of stable isotope data indexed according to depths of samples under present sea level (elevation). (b) Cross plot of stable isotope data indexed according to depths of samples below the sea floor (burial).

TABLE CAPTIONS

Table 1. U-series and radiocarbon ages of older Pleistocene (pre-LGM) samples. Detailed data will be published elsewhere.

Table 2. Microfacies of investigated older Pleistocene samples. Delineation was made based on tree diagram of a cluster analysis (Fig. 4). Sequence of samples is according to appearance in dendrogram of cluster analysis (Fig. 4).

Table 3. Cement distribution in the holes. Percentages sum up to total values of marine and meteoric cements as shown in Table 2.

Table 4. Mineralogy and geochemistry of the investigated samples. QTZ = quartz; ARA = aragonite; HMC = high-magnesium calcite; LMC = low-magnesium calcite.

Table 5. Correlation matrix based on the composition of samples including depth below sea level, i.e., elevation. R-values are plotted in the lower left (statistically significant correlations marked bold) and p-values in the upper right parts of the table.

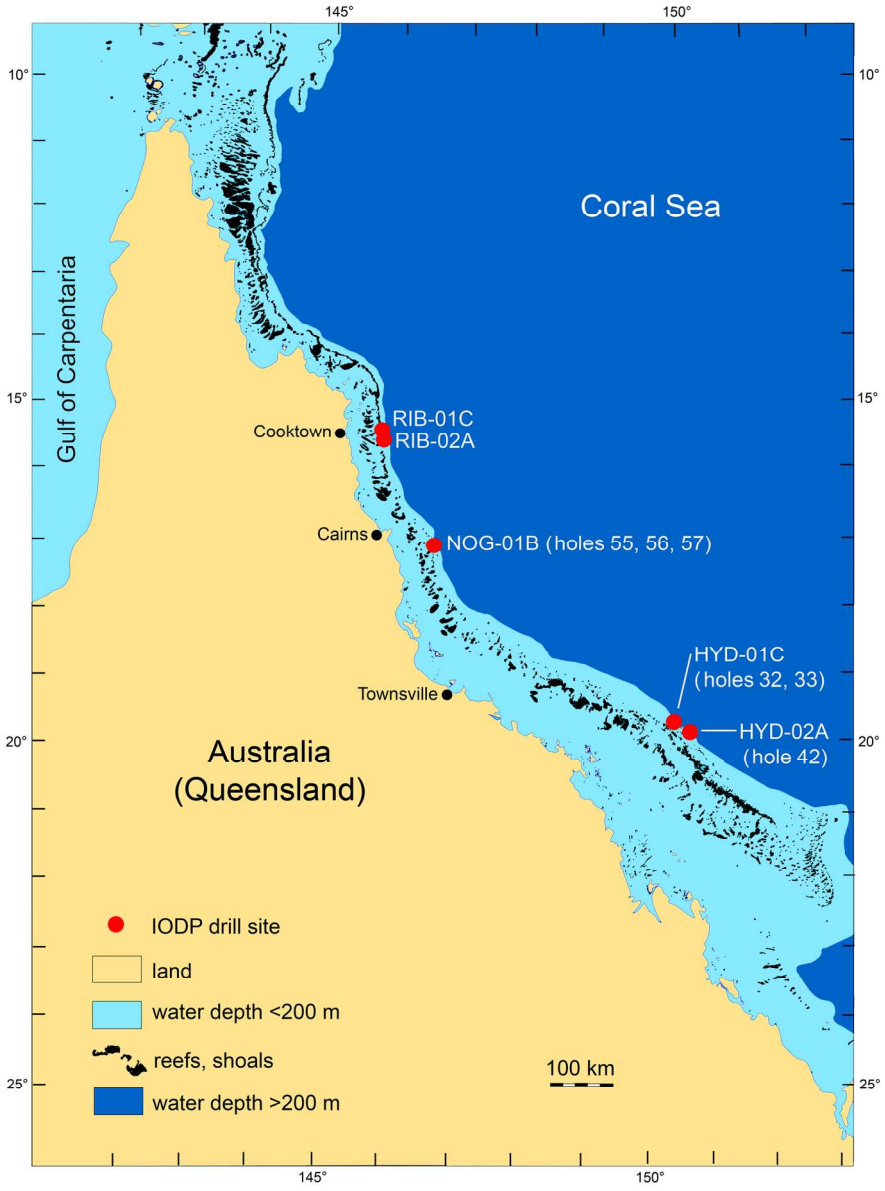

Fig. 1. Drill locations including investigated holes of IODP Expedition 325 along the Great Barrier Reef (reefs and shoals in black). Reefs and shoals on Queensland Plateau east of Cairns (Coral Sea) are not shown. RIB = Ribbon Reef; NOG = Noggin Pass; HYD = Hydrographer's Passage. Map modified from Purdy and Winterer (2006, their Fig. 13).
150x199mm (300 x 300 DPI)

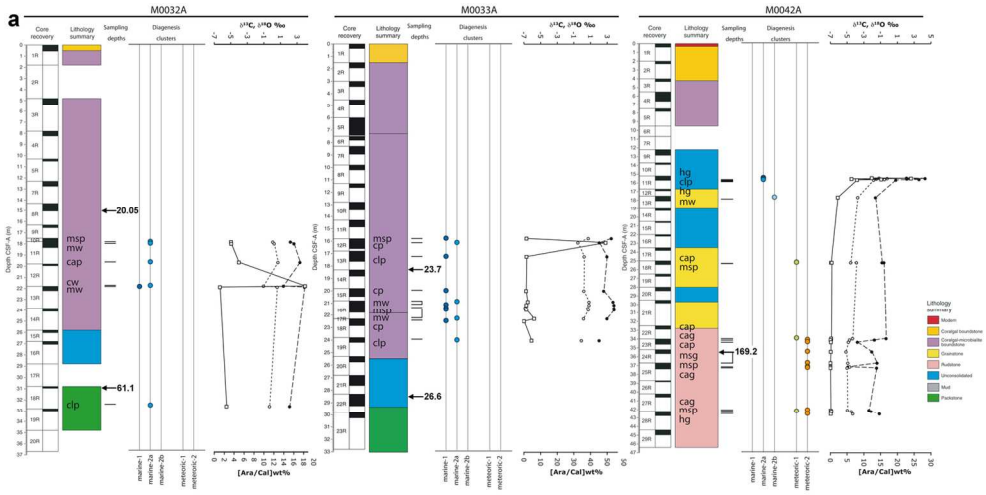

Fig. 2. (a) Core logs of holes M0032A, M0033A, and M0042A. (b) Core logs of holes M0055A, M0056A, and M0057A. Lithologies are taken from Webster et al. (2011). Microfacies delineated during this study are shown using abbreviations in the text. To the right of the columns, diagenesis from cluster analysis (Fig. 9), isotope geochemistry (open circles for δ18O and closed circles for δ13C), mineralogy (open squares), and chronology data are plotted. Ara/Cal = ratio of aragonite and calcite abundances. Stable isotope data also shown on figure 7.
138x70mm (300 x 300 DPI)

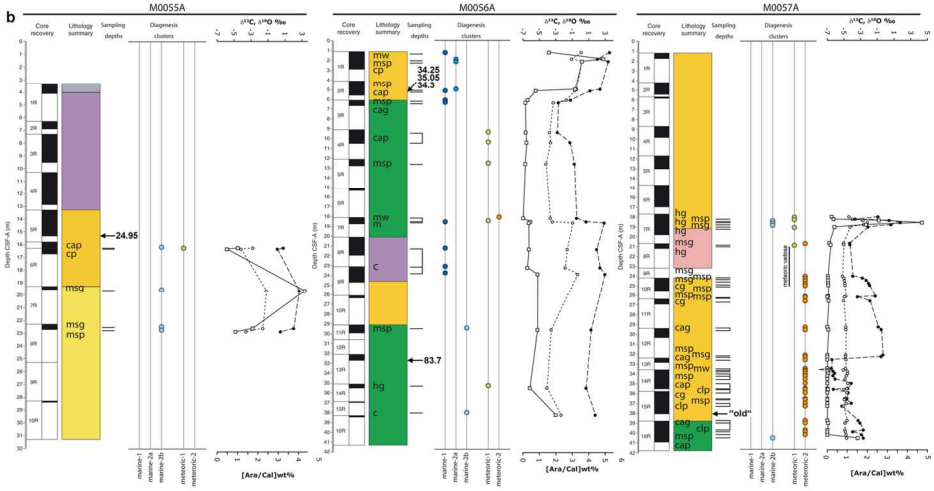

Fig. 2. (a) Core logs of holes M0032A, M0033A, and M0042A. (b) Core logs of holes M0055A, M0056A, and M0057A. Lithologies are taken from Webster et al. (2011). Microfacies delineated during this study are shown using abbreviations in the text. To the right of the columns, diagenesis from cluster analysis (Fig. 9), isotope geochemistry (open circles for δ18O and closed circles for δ13C), mineralogy (open squares), and chronology data are plotted. Ara/Cal = ratio of aragonite and calcite abundances. Stable isotope data also shown on figure 7.
140x73mm (300 x 300 DPI)

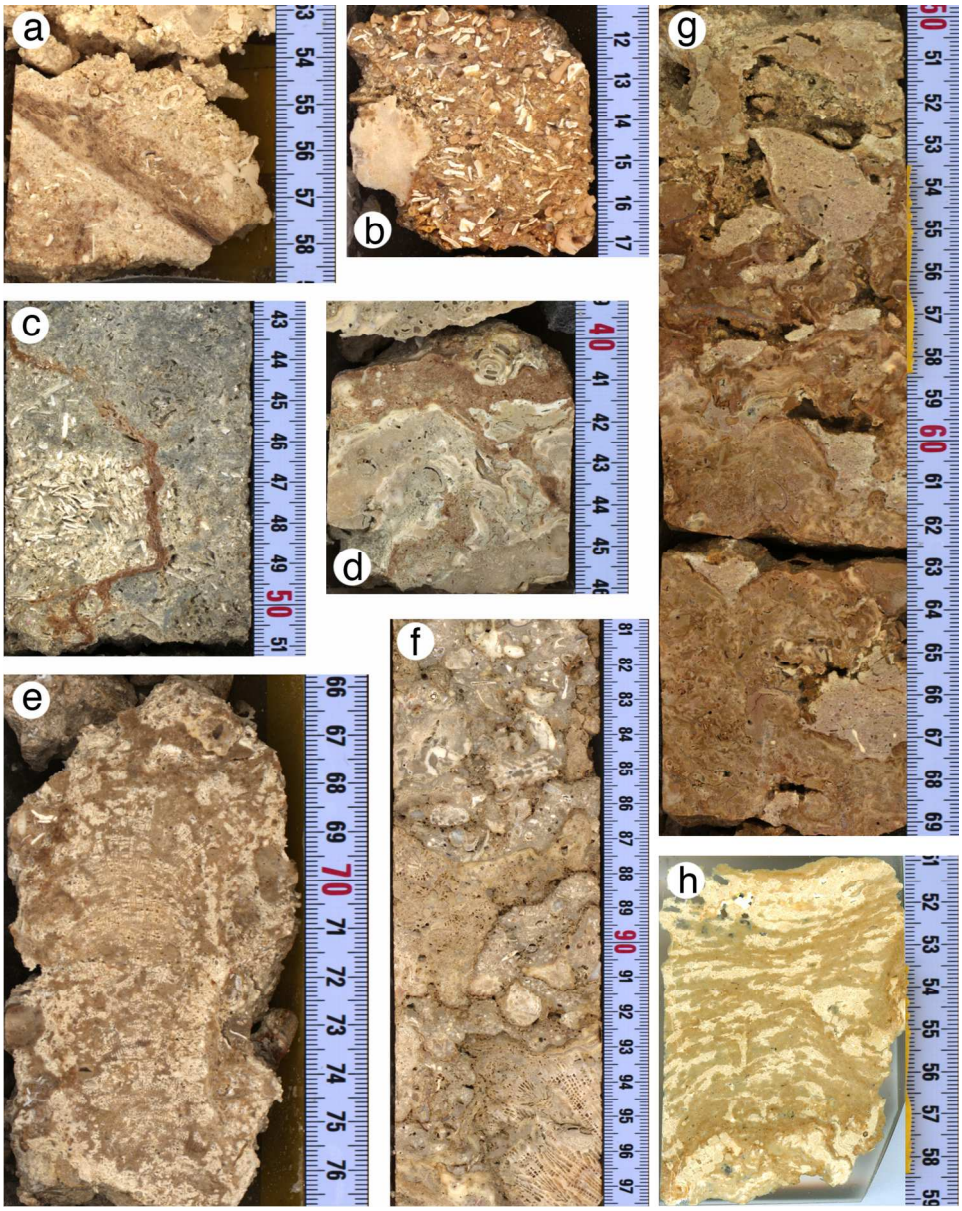

Fig. 3. Photographs of older Pleistocene hand specimens. (a) Coralline algal grainstone with rhizolith (brown). Hole 42, core 25, 54-59 cm; ca. 88 m below sea level (SL). (b) Halimeda grainstone. Hole 55, core 7, 11-17 cm; ca. 107 m below SL. (c) Halimeda grainstone with coral fragment and thin caliche (brown). Hole 57, core 7, 38-51 cm; ca. 61 m below SL. (d) Caliche (brown) in coral-algal packstone. Hole 57, core 13; ca. 115 m below SL. (e) Diagenetically altered faviid(?) coral. Hole 55, core 6, 66-77 cm; ca. 115 m below SL. (f) Coral grainstone with clear signs of meteoric alteration. Hole 56, core 2, 81-98 cm; ca. 86 m below SL. (g) Mixed skeletal packstone with dissolution cavities that are partially filled by fine-grained internal sediment. Hole 57, core 14-R2, 48-70 cm; ca. 77 m below SL. (h) Altered microbialite, reminescent of zebra limestone. Hole 57, core 7, 52-59 cm; ca. 100 m below SL.
180x226mm (300 x 300 DPI)

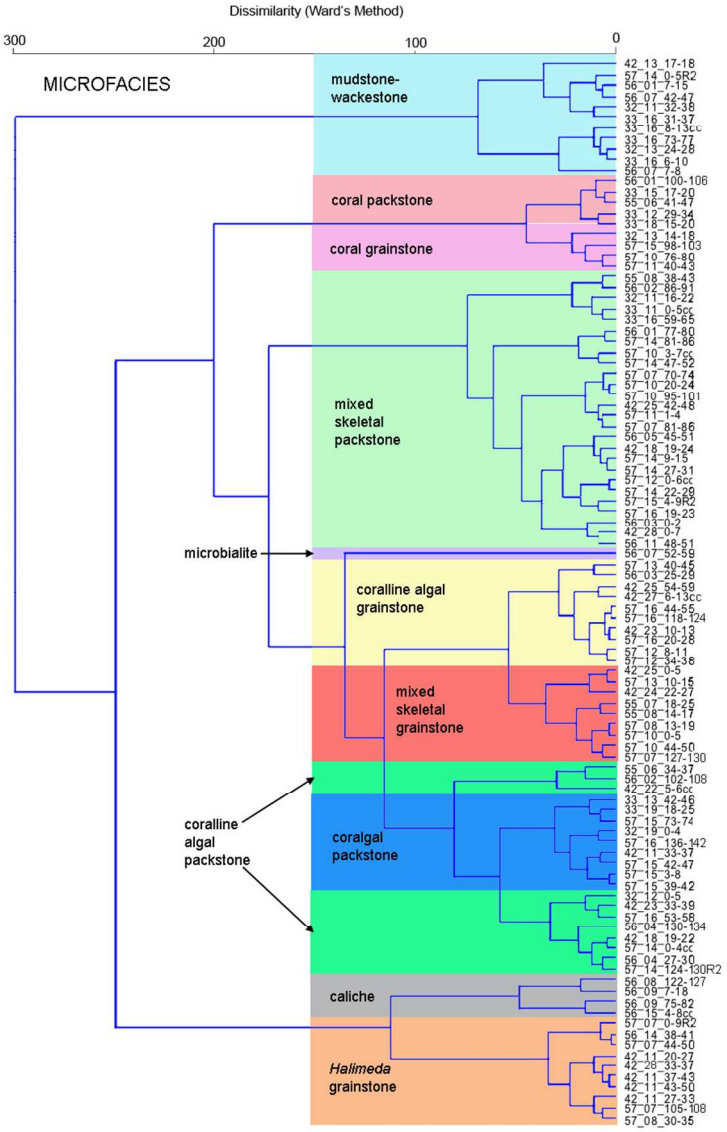

Fig. 4. Tree diagram of a cluster analysis (Ward's method) based on abundance data of constituent particles produces eleven microfacies. Ward's algorhithm was used because it exhibited the most meaningful results.
179x269mm (140 x 140 DPI)

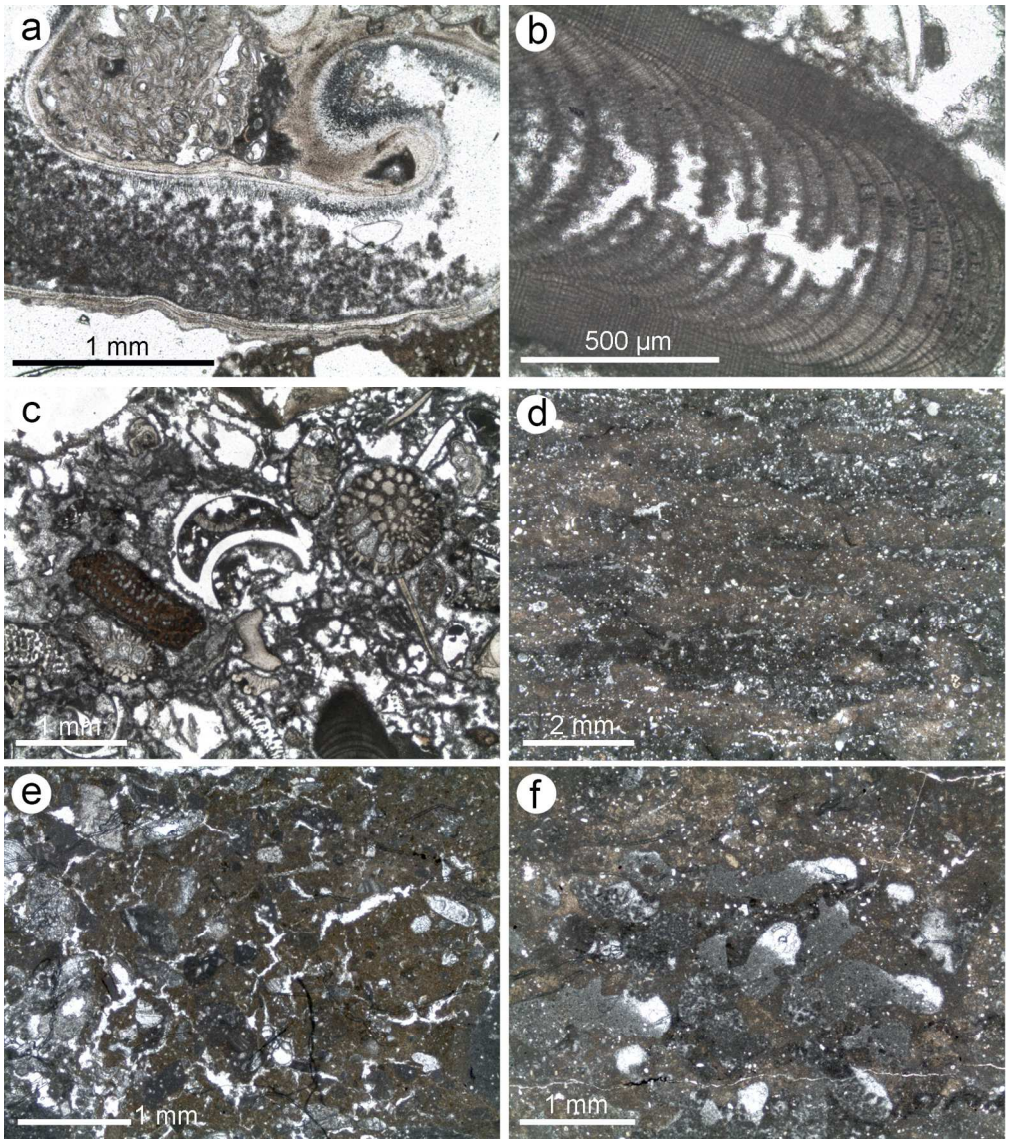

Fig. 5. Thin-section micrographs showing microfacies and marine and meteoric diagenesis. (a) Mixed skeletal packstone. Gastropod shell lined on inner side with aragonite needle cement; peloidal cement fills most of the inner shell. Hole 33, core 16, 59-65 cm. (b) Coralline algal grainstone. Partly dissolved and neomorphosed coralline algal fragment. Blocky cement lines dissolved cavity. Hole 42, core 23, 10-13 cm. (c) Coralline algal packstone with mollusk shells, Halimeda, and coral fragments. Note dissolution of gastropod shells (mouldic porosity). Hole 42, core 23, 10-13 cm. (d) Microbialite that shows irregular lamination. Note abundant small cavities and incorporation of small skeletal fragments. Hole 56, core 7, 52-59 cm. (e) Caliche developed within mixed skeletal packstone, with mottled texture and brecciation. Hole 57, core 14, 81-86 cm. (f) Caliche with possible diagenetic geopetals. Hole 56, core 9, 7-18 cm.
161x182mm (300 x 300 DPI)

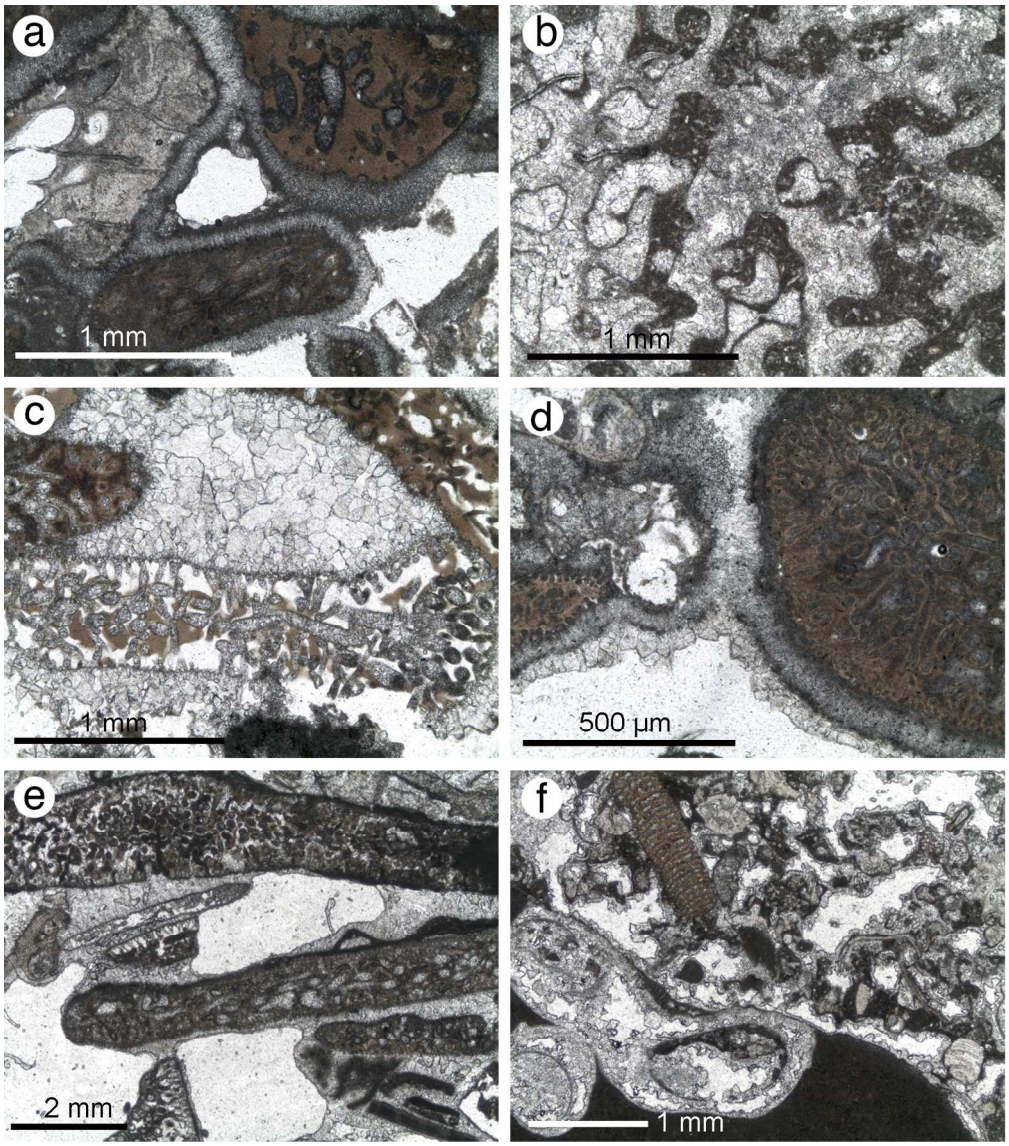

Fig. 6. Thin-section micrographs exhibiting microfacies and marine and meteoric diagenesis. (a) Halimeda grainstone. Halimeda and coral fragments with marine acicular cement and meteoric blocky cement. Note that micrite envelopes occur on grains boundaries and on marine cements. Hole 42, core 11, 27-33 cm. (b) Halimeda grainstone. Neomorphosed coral with interparticle porosity filled by microcrystalline, peloidal, and blocky cements. Hole 42, core 28, 33-37 cm. (c) Halimeda grainstone. Neomorphosed and partly dissolved Halimeda fragments and blocky and dogtooth cements in packstone. Hole 56, core 14, 38-41 cm. (d) Halimeda grainstone. Halimeda and other biogenic fragments with acicular (marine) and dogtooth (meteoric) cements. Note micrite envelopes on marine cement fringe. Core 57, barrel 7, 105-108 cm. (e) Halimeda grainstone. Halimeda fragments with blocky cement and meniscus texture (meteoric vadose environment) in grainstone. Hole 57, core 8, 30-35 cm. (f) Mixed skeletal grainstone. Biogenic fragments in boundstone that shows strong signs of dissolution. Fragment in lower left corner is coralline alga. Pores lined with blocky and dogtooth (scalenohedral) cements. Hole 57, core 13, 10-15 cm.
151x172mm (300 x 300 DPI)

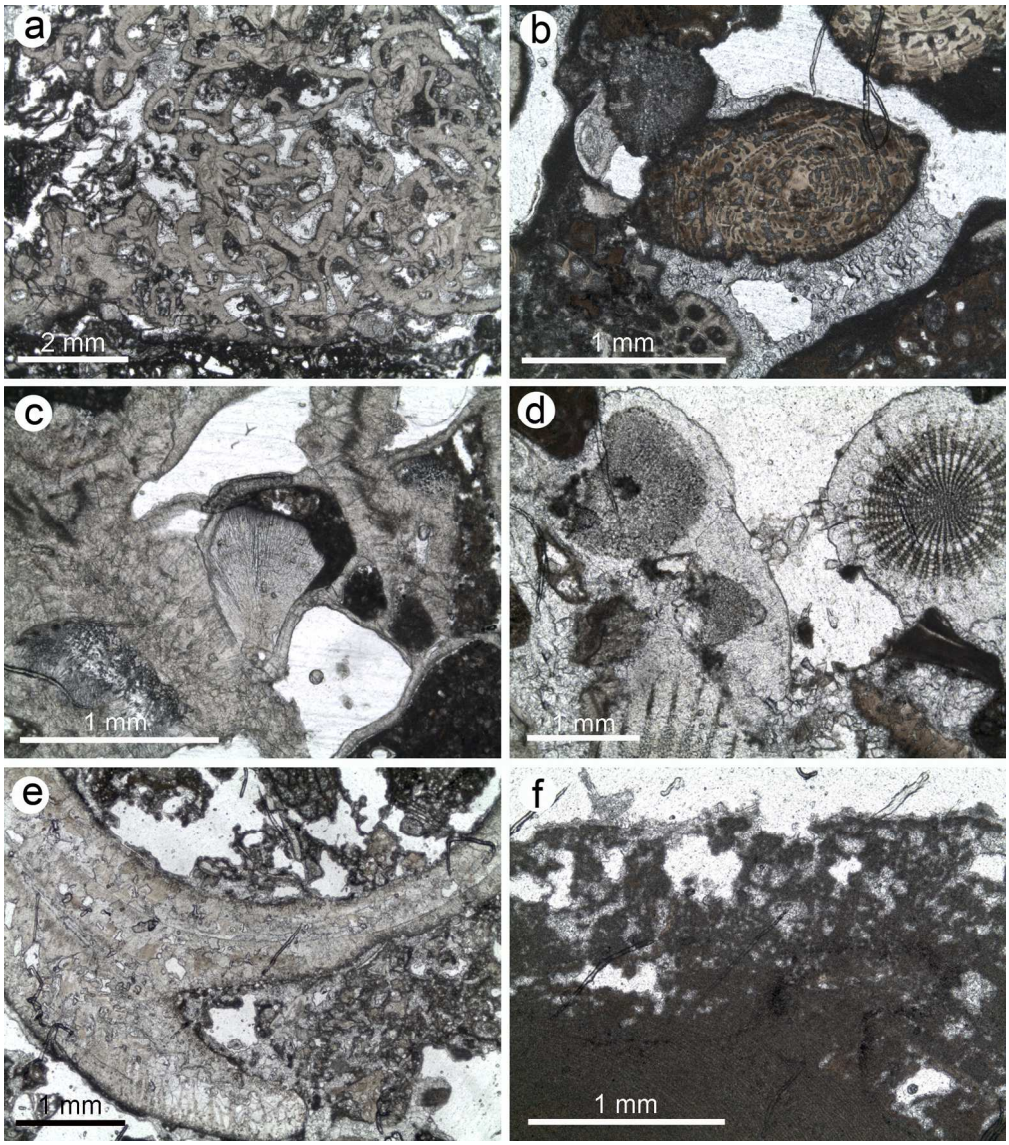

Fig. 7. Thin-section micrographs exhibiting microfacies and marine and meteoric diagenesis. (a) Coralline algal grainstone. Encrusting foraminifer (Carpenteria sp.) with blocky cement in intraskeletal porosity. Hole 42, core 25, 54-59 cm. (b) Coral-algal packstone. Benthic foraminifer with micrite envelope and cemented by blocky spar. Hole 42, core 11, 33-37 cm. (c) Coral grainstone. Botryoidal (center) and needle (lower left) cement in primary porosity of coral. Hole 32, core 13, 14-18 cm. (d) Mixed skeletal grainstone. Syntaxial cement around echinoid spines. Hole 55, core 7, 18-25 cm. (e) Mixed skeletal packstone. Mollusk shell that is neomorphosed to blocky spar. Hole 42, core 25, 42-28 cm. (f) Coralline algal grainstone. Algal fragment that towards the top is altered to peloidal texture. Hole 42, core 25, 54-59 cm.
161x182mm (300 x 300 DPI)

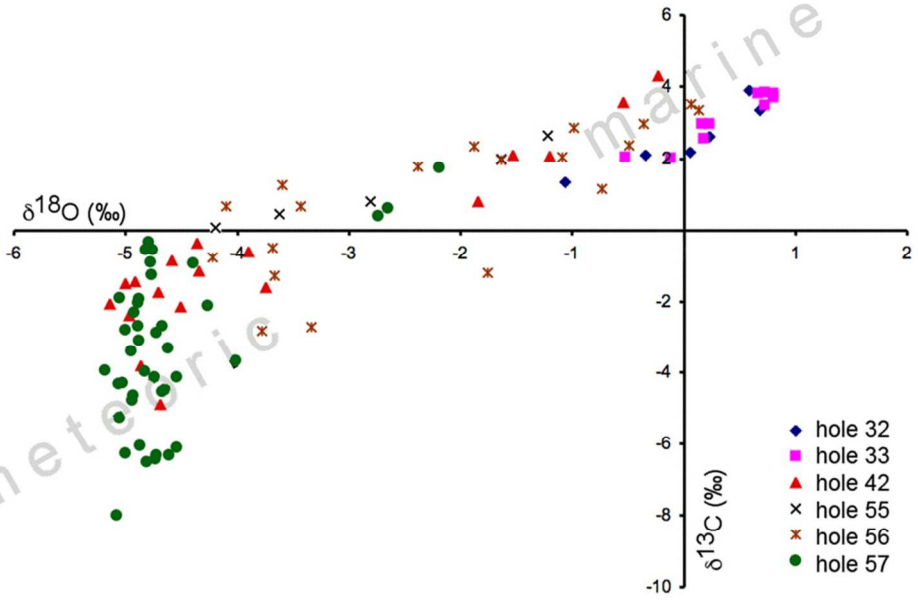

Fig. 8. Oxygen and carbon isotope values of older Pleistocene (pre-LGM) samples. Typical marine samples plot in the slightly positive area of the graph; samples under the influence of meteoric diagenesis plot in the negative quadrant of the graph.
220x142mm (119 x 119 DPI)

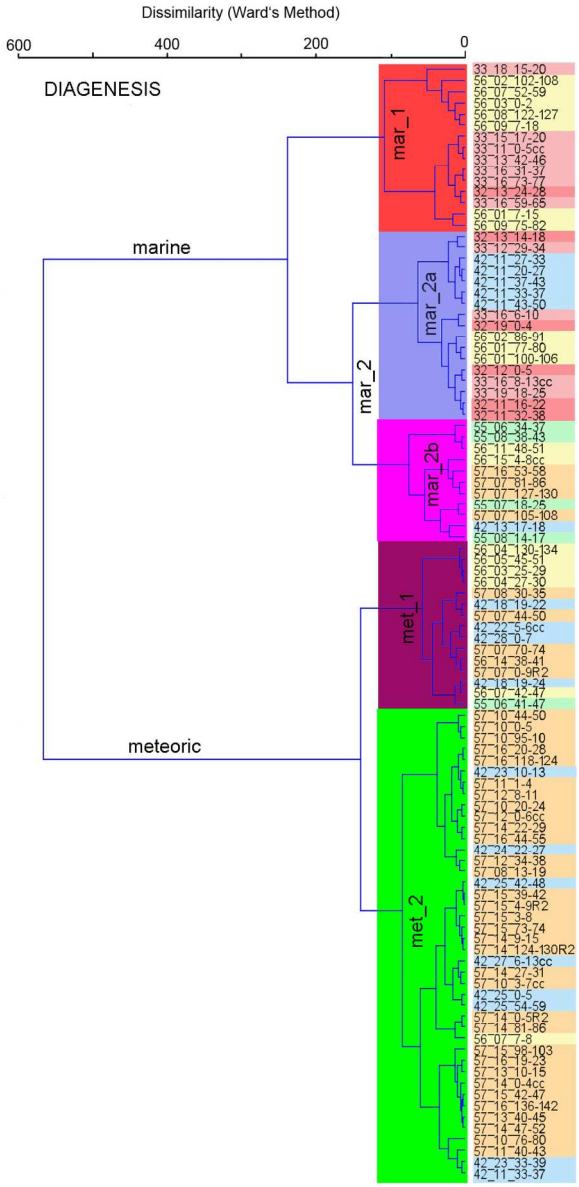

Fig. 9. Tree diagram of a cluster analysis (Ward's method) based on diagenesis, mineralogy, and stable isotope geochemistry data. Ward's algorhithm was used because it produced the most meaningful results.
179x364mm (300 x 300 DPI)

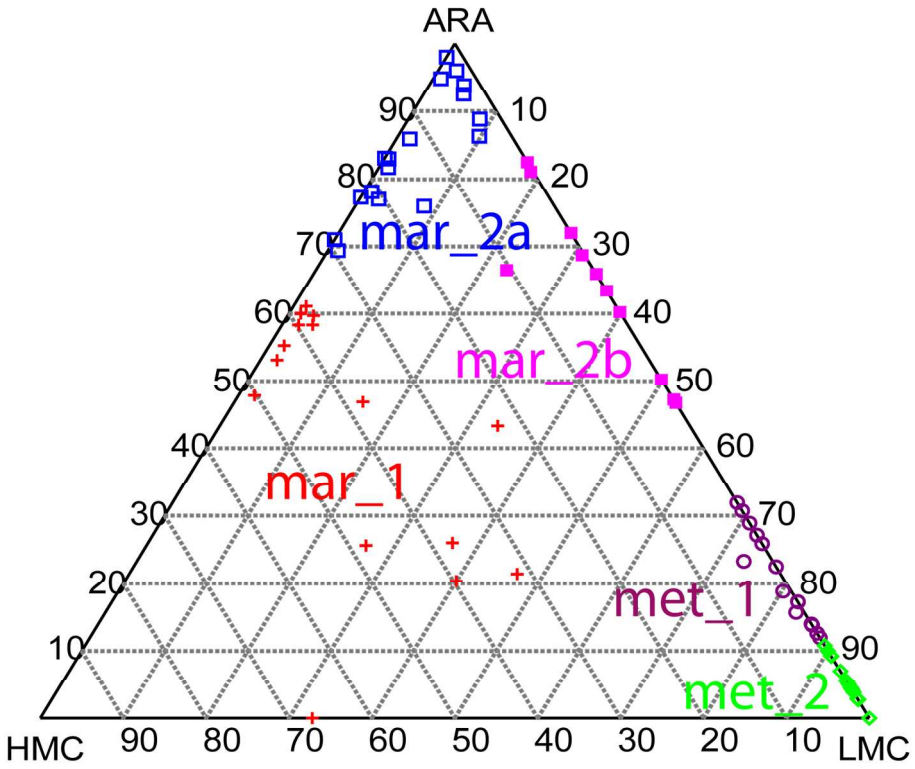

Fig. 10. Ternary diagram of carbonate mineralogy with samples highlighted according to membership in diagenetic sub-clusters in Figure 9. ARA = aragonite; LMC = low-magnesium calcite; HMC = high-magnesium calcite.
152x119mm (300 x 300 DPI)

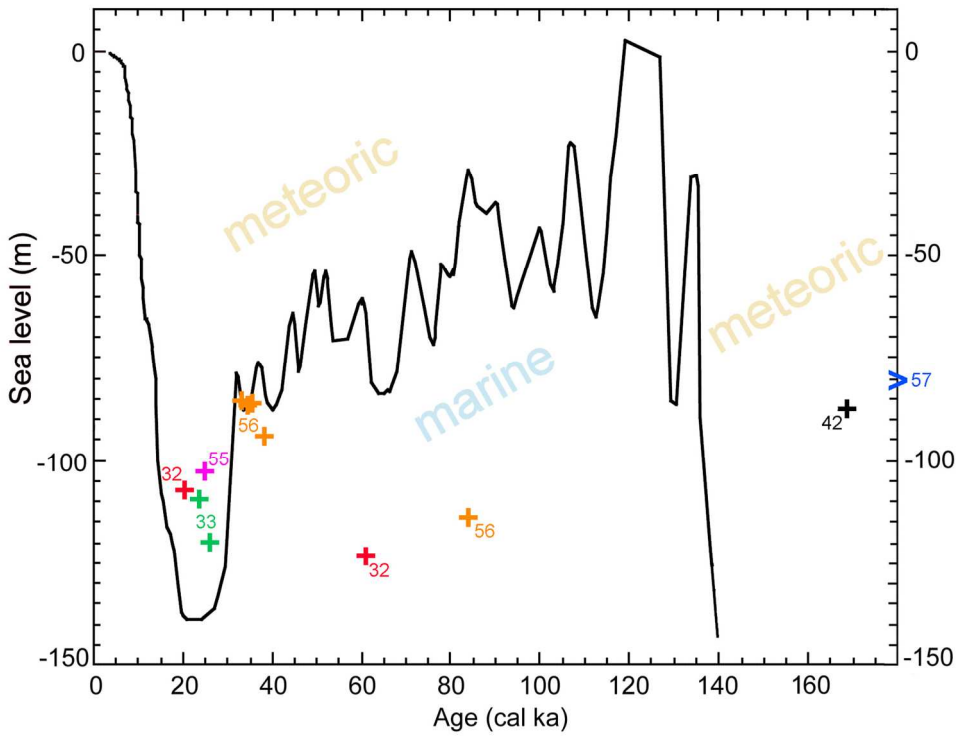

Fig. 11. U/Th-series ages of from older Pleistocene (pre-LGM) samples plotted on late Pleistocene sea-level data from the Huon Peninsula, New Guinea, and the Bonparte Gulf, Australia (Yokoyama and Esat, 2011). The isostatic influence on local deglacial sea level is estimated to be in the order of max. 20-25 m (Yokoyama et al., 2006). Sea-level data older than 140 kyrs BP is not plotted.
220x166mm (229 x 229 DPI)

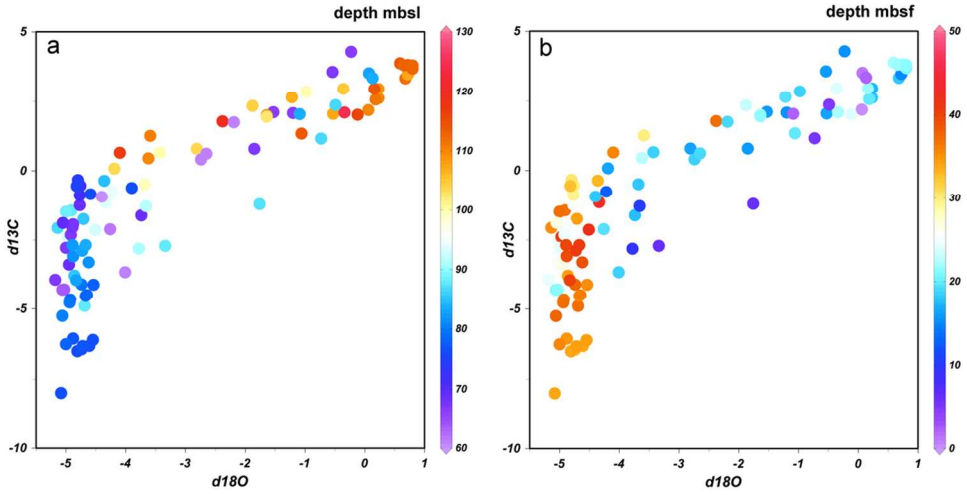

Fig. 12. (a) Cross plot of stable isotope data indexed according to depths of samples under present sea level (elevation). (b) Cross plot of stable isotope data indexed according to depths of samples below the sea floor (burial).
113x58mm (300 x 300 DPI)

sample ID	hole depth	depth in hole	sample elevation	Method	age max	age min	error on U-Th max
	mbsl	m	mbsl		kyr BP	kyr BP	kyr
32-8R cc 0-2	91.9	15.05	106.95	U-Th Pre	20.4	19.7	0.24
32-18R cc 8-10	91.9	30.96	122.86	U-Th Pre	61.1	61.1	0.8
33-14R 0-6	91.3	18.34	109.64	U-Th Post	23.7	23.7	0.10
33-22R 24-26	91.3	28.55	119.85	U-Th Post	26.7	26.5	0.13
42-24R cc 8-9	50.8	35.66	86.46	U-Th Pre	169.3	169.2	4.5
55-5R cc 0-1	87.3	15.33	102.63	U-Th Pre	25.1	24.8	0.3
56-2R 90-95	81.2	5.02	86.22	U-Th Post	34.3	34.2	0.3
56-2R 124-128	81.2	5.35	86.55	U-Th Post	35.6	34.5	0.3
56-2R cc 149-150	81.2	5.59	86.79	C14 Pre	34.7	33.9	
56-5R cc 68-69	81.2	12.78	93.98	C14 Pre	39.3	38.0	
56-13R cc 2-3	81.2	32.70	113.9	U-Th Pre	84.1	83.3	1.1
57-15R cc 9-10	42.3	38.05	80.35	U-Th Pre	old		

sample ID	IODP sample identifier, cc indicate a core catcher sample
hole depth	water depth in which each hole was drilled
depth in hole	depth from the sea floor to the sample down-hole
sample elevation	depth of each sample below present sea level
Method	method of age determination: uranium-thorium, or radiocarbon. Pre indicates "shipboard" measurements made prior to the OSP in Bremen, Post indicates new measurements
age max	for U-Th this is the closed system age determination with no correction for initial 230Th, for C14 this is the upper limit of the 95% confidence interval of the calibrated age (calibration details in the IODP proceedings)
age min	for U-Th thus is a closed system age determination with a correction for initial 230Th based on a contaminant being of crustal composition (IODP proceedings for details), for C14 this is the upper limit of the 95% confidence interval of the calibrated age (calibration details in the IODP proceedings)
error on U-Th max	this is the error arrising from analyitical uncertainty of the U-Th age with no correction for initial 230Th

sample	coral %	cor. alga %	Halimeda %	mollusk %	foram benth %	foram encr %	echino %	peloid %	microbialite %	caliche %	prim. poro. %	sec. poro. %	marine cement	meteoric cement	matrix %
1 Mixed skeletal packstone (msp)															
55_08_38-43	15.0	10.0	3.0	10.5	5.0	1.0	1.0	0.0	0.0	0.0	1.5	16.0	1.0	10.5	25.5
56_02_86-91	15.5	15.5	1.5	16.0	2.5	4.5	2.0	0.0	0.0	0.0	2.5	4.5	6.5	0.0	29.0
32_11_16-22	11.0	8.5	0.5	5.0	6.5	13.0	0.0	1.0	0.0	0.0	3.0	0.0	13.5	0.0	38.0
33_11_0-5cc	23.5	1.5	0.0	8.0	1.5	7.5	0.0	0.0	0.0	0.0	3.5	0.0	18.5	0.5	35.5
33_16_59-65	19.5	8.5	1.0	4.5	3.5	10.0	1.0	1.5	0.0	0.0	5.5	1.0	9.0	0.0	35.0
56_01_77-80	11.5	9.0	1.0	2.0	0.5	1.0	0.0	1.0	0.0	18.5	0.0	8.0	13.5	2.5	31.5
57_14_81-86R2	8.5	5.0	0.5	4.0	2.0	0.5	0.0	0.5	0.0	24.5	0.5	11.0	2.0	11.5	29.5
57_10_3-7cc	5.5	16.5	1.5	0.0	3.5	2.5	0.0	0.0	0.0	8.5	0.0	19.0	3.0	18.5	21.5
57_14_47-52R2	1.0	9.5	1.5	1.5	7.5	0.0	0.0	1.0	0.0	16.0	0.0	9.0	0.5	28.5	24.0
57_07_70-74	1.0	3.5	9.5	6.0	7.5	0.5	1.0	0.5	0.0	0.0	0.5	20.5	2.0	26.0	21.5
57_10_20-24	0.5	1.5	9.0	3.0	5.5	0.5	1.0	0.0	0.0	0.0	0.5	25.0	1.5	34.5	17.5
57_10_95-101	1.0	3.0	11.5	4.5	7.5	0.0	1.0	0.0	0.0	0.0	1.0	34.0	2.0	21.0	13.5
42_25_42-48	5.0	7.0	3.5	6.0	6.5	0.0	2.0	5.0	0.0	0.0	1.5	16.5	3.0	26.5	17.5
57_11_1-4	6.0	3.5	6.0	3.5	2.5	0.0	0.0	0.0	0.0	3.0	0.0	20.0	2.0	32.5	21.0
57_07_81-86	9.0	8.5	8.0	2.0	4.5	0.0	0.5	0.0	0.0	0.0	0.0	16.5	6.5	29.0	15.5
56_05_45-51	1.0	10.0	2.5	5.5	11.0	2.0	3.5	0.0	0.0	2.0	1.0	20.5	0.0	6.0	35.0
42_18_19-24	8.0	2.5	6.5	5.5	9.0	0.0	2.0	1.0	0.0	0.0	0.0	21.0	0.0	12.0	32.5
57_14_9-15	3.5	8.5	7.5	2.5	10.0	2.5	2.5	0.5	0.0	0.0	0.0	10.0	1.0	19.0	32.5
57_14_27-31	2.0	5.0	5.0	5.0	8.5	2.0	0.5	0.0	0.0	0.0	1.5	16.5	2.0	23.0	29.0
57_12_0-6cc	3.0	7.5	2.4	1.2	4.3	0.0	1.2	0.0	0.0	0.0	0.0	25.6	0.0	27.4	27.4
57_14_22-29R2	4.0	3.5	4.0	1.5	2.5	2.0	0.5	1.5	0.0	0.0	0.0	23.5	1.5	27.5	28.0
57_15_4-9R2	0.0	7.5	1.0	3.5	3.0	11.5	0.5	0.5	0.0	0.0	0.0	14.5	1.5	25.5	31.0
57_16_19-23R2	1.5	9.5	0.5	2.5	1.0	17.5	0.0	1.0	0.0	0.0	0.0	12.5	5.0	29.0	20.0
56_03_0-2	6.5	17.5	15.5	7.0	6.5	5.5	4.0	0.0	0.0	2.5	1.5	8.0	0.0	1.0	24.5
42_28_0-7	5.5	7.0	15.5	3.5	5.0	1.0	0.5	4.0	0.0	0.0	0.5	13.5	3.0	16.0	25.0
56_11_48-51	0.0	6.0	18.5	6.0	7.0	0.0	1.0	0.0	0.0	0.0	0.0	21.0	0.0	6.5	34.0
mean	**6.5**	**7.5**	**5.3**	**4.6**	**5.2**	**3.3**	**1.0**	**0.7**	**0.0**	**2.9**	**0.9**	**14.9**	**3.8**	**16.7**	**26.7**
2 Mixed skeletal grainstone (msg)															
42_25_0-5	0.5	18.0	1.0	6.0	17.0	1.5	1.0	5.5	0.0	0.0	1.0	23.5	7.5	17.5	0.0
57_13_10-15	1.0	21.5	1.0	1.5	19.0	3.5	0.0	4.0	0.0	0.0	0.5	12.5	1.0	34.0	0.5
42_24_22-27	1.5	6.5	4.0	9.0	16.5	3.0	0.5	6.0	0.0	0.0	0.0	11.5	3.5	38.0	0.0
55_07_18-25	7.0	16.0	8.5	9.0	3.0	4.0	3.0	2.0	0.0	0.0	6.5	3.0	16.5	19.5	2.0
55_08_14-17	10.5	6.5	11.5	7.5	3.5	0.5	6.0	1.0	0.0	0.0	5.0	6.0	29.5	11.5	1.0
57_08_13-19	1.5	5.5	10.5	3.0	8.5	0.0	0.5	0.0	0.0	0.0	1.5	24.0	3.0	42.0	0.0
57_10_0-5	1.5	4.5	6.0	4.0	8.0	0.5	1.5	0.0	0.0	0.0	2.0	38.0	3.0	31.0	0.0
57_10_44-50	0.5	4.5	13.5	4.5	5.5	0.0	0.0	0.0	0.0	0.0	0.0	30.0	2.5	34.0	5.0
57_07_127-130	1.0	12.0	13.5	4.0	4.0	1.0	1.0	0.0	0.0	0.0	1.0	14.0	3.5	35.5	9.5
mean	**2.8**	**10.6**	**7.7**	**5.4**	**9.4**	**1.6**	**1.5**	**2.1**	**0.0**	**0.0**	**1.9**	**18.1**	**7.8**	**29.2**	**2.0**
3 Mudstone-wackestone (mw)															
42_13_17-18	0.0	0.0	31.5	10.5	11.0	0.0	0.5	0.0	0.0	0.0	0.0	2.0	0.0	1.5	43.0
57_14_0-5R2	2.5	3.5	12.5	3.0	5.0	2.0	1.5	2.5	0.0	1.0	0.5	6.0	0.0	13.5	46.5
56_01_7-15	4.0	9.0	6.0	1.0	1.5	1.0	0.0	1.0	0.0	0.0	0.0	14.0	4.5	15.0	43.0
56_07_42-47	1.0	7.0	3.5	3.5	7.0	2.5	4.0	0.0	0.0	1.5	0.0	21.0	0.0	4.0	45.0
32_11_32-38	14.0	8.5	2.5	3.0	7.0	1.0	0.5	0.5	0.0	0.0	0.5	0.0	9.0	0.0	53.5

33_16_31-37	3.0	10.0	0.0	6.0	3.5	5.5	1.0	0.0	0.0	0.0	5.0	0.0	4.5	0.0	61.5
33_16_8-13cc	1.0	0.0	0.5	4.0	5.0	0.0	0.0	9.0	0.0	0.0	4.0	2.0	0.0	0.0	74.5
33_16_73-77	0.5	0.0	2.5	5.5	10.5	2.0	0.0	4.0	0.0	0.0	6.5	1.0	0.0	0.0	67.5
32_13_24-28	1.5	0.5	1.5	1.5	7.5	6.0	0.0	2.5	0.0	0.0	4.5	0.0	4.0	0.0	70.5
33_16_6-10	2.5	0.5	1.5	0.5	8.5	1.5	0.5	2.5	0.0	0.0	5.0	0.0	1.5	0.5	75.0
56_07_7-8	0.0	0.0	0.0	0.0	0.0	0.0	0.0	0.0	0.0	0.0	0.0	0.0	0.0	0.0	100.0
mean	**2.7**	**3.5**	**5.6**	**3.5**	**6.0**	**2.0**	**0.7**	**2.0**	**0.0**	**0.2**	**2.4**	**4.2**	**2.1**	**3.1**	**61.8**
4 Coral packstone (cp)															
56_01_100-106	28.5	10.5	2.0	0.0	0.5	0.5	0.0	0.0	0.0	7.5	1.5	10.0	14.5	3.0	21.5
33_15_17-20	32.0	8.0	0.5	1.5	2.0	5.5	0.0	0.0	0.0	0.0	4.5	0.0	22.0	0.0	24.0
55_06_41-47	33.0	8.0	0.5	3.0	2.0	0.0	1.0	0.5	0.0	0.0	2.5	11.0	13.0	8.0	17.5
33_12_29-34	36.5	7.5	2.0	2.0	3.0	0.5	2.0	0.0	0.0	0.0	6.0	0.0	9.0	0.0	31.5
33_18_15-20	42.5	9.5	0.0	0.0	2.0	0.5	0.0	0.5	0.0	0.0	4.5	0.0	19.5	0.0	21.0
mean	**34.5**	**8.7**	**1.0**	**1.3**	**1.9**	**1.4**	**0.6**	**0.2**	**0.0**	**1.5**	**3.8**	**4.2**	**15.6**	**2.2**	**23.1**
5 Coral grainstone (cg)															
32_13_14-18	51.5	2.5	0.0	0.0	0.0	0.5	0.0	0.0	0.0	0.0	17.5	0.0	25.5	0.0	2.5
57_15_98-103	32.0	16.5	0.0	0.0	0.0	0.0	0.0	0.0	0.0	0.0	0.0	8.5	11.0	32.0	0.0
57_10_76-80	39.5	0.0	0.0	0.0	0.0	0.0	0.0	0.0	0.0	0.0	0.0	9.0	27.0	24.5	0.0
57_11_40-43	30.5	0.0	0.0	2.0	0.5	0.0	0.0	0.0	0.0	0.0	26.0	2.5	6.0	32.5	0.0
mean	**38.4**	**4.8**	**0.0**	**0.5**	**0.1**	**0.1**	**0.0**	**0.0**	**0.0**	**0.0**	**10.9**	**5.0**	**17.4**	**22.3**	**0.6**
6 Coralline algal grainstone (cag)															
57_13_40-45	8.0	27.5	0.0	1.5	3.0	0.0	0.0	3.0	0.0	0.0	1.5	9.5	5.0	30.5	10.5
56_03_25-29	2.0	27.0	1.5	12.0	10.0	4.0	2.0	2.5	0.0	0.0	2.0	22.0	0.0	0.0	15.0
42_25_54-59	4.0	21.0	1.0	3.0	11.5	9.5	1.0	7.0	0.0	0.0	1.5	19.0	2.0	15.5	4.0
42_27_6-13cc	2.0	27.5	4.0	3.5	10.5	0.5	0.0	6.0	0.0	0.0	1.0	23.5	1.5	19.0	1.0
57_16_44-55	1.5	22.5	1.0	3.0	7.0	2.0	1.0	0.5	0.0	0.0	0.0	21.5	4.5	34.5	1.0
57_16_118-124	1.5	22.5	1.0	4.0	4.0	3.5	1.0	2.0	0.0	0.0	0.0	21.5	5.0	32.0	2.0
42_23_10-13	1.5	20.5	1.5	2.5	7.0	1.0	0.0	1.0	0.0	0.0	0.5	17.5	4.0	39.0	4.0
57_16_20-28	0.5	19.0	0.5	3.0	5.5	4.5	0.0	0.0	0.0	0.0	0.5	22.5	4.0	36.5	3.5
57_12_8-11	6.5	14.5	1.5	3.5	5.0	1.0	2.0	0.0	0.0	0.0	2.0	20.0	1.5	36.0	6.5
57_12_34-38	10.5	16.0	1.0	4.0	3.0	0.0	0.5	0.0	0.0	0.0	1.0	23.5	0.0	38.0	2.5
mean	**3.8**	**21.8**	**1.3**	**4.0**	**6.7**	**2.6**	**0.8**	**2.2**	**0.0**	**0.0**	**1.0**	**20.1**	**2.8**	**28.1**	**5.0**
7 Coral-algal packstone (cp)															
33_13_42-46	20.0	28.5	1.0	2.0	4.0	10.0	0.0	0.0	0.0	0.0	5.0	0.0	14.5	0.0	15.0
33_19_18-25	15.0	22.0	6.0	1.0	6.5	4.5	0.0	0.0	0.0	0.0	9.0	0.0	12.5	0.0	23.5
57_15_73-74R2	10.0	25.5	0.0	1.0	1.0	4.5	0.0	0.0	0.0	0.0	0.0	14.5	2.5	20.0	21.0
32_19_0-4	25.5	18.0	5.5	2.5	3.5	0.0	2.0	0.0	0.0	0.0	5.5	0.0	19.0	0.5	18.0
57_16_136-142	26.5	24.5	0.5	0.0	1.5	0.5	0.0	0.0	0.0	0.0	0.5	6.5	3.0	28.0	9.0
42_11_33-37	14.0	16.5	1.0	4.0	10.5	1.0	0.5	1.5	0.0	0.0	0.0	5.5	6.0	25.5	14.0
57_15_42-47R2	18.0	17.0	1.0	1.0	2.0	6.0	1.0	1.5	0.0	0.0	0.0	7.0	3.0	30.0	12.5
57_15_3-8	17.5	10.5	1.5	2.0	2.5	2.0	0.0	1.5	0.0	0.0	3.0	9.0	1.0	26.5	23.0
57_15_39-42	17.0	14.5	1.0	0.0	2.0	1.5	0.0	0.0	0.0	0.0	0.5	16.0	0.0	24.0	23.5
mean	**18.2**	**19.7**	**1.9**	**1.5**	**3.7**	**3.3**	**0.4**	**0.5**	**0.0**	**0.0**	**2.6**	**6.5**	**6.8**	**17.2**	**17.7**

8 Coralline algal packstone (cap)

55_06_34-37	6.0	44.5	0.0	6.5	1.0	10.5	0.0	0.0	0.0	0.0	2.5	4.0	9.5	7.5	8.0
56_02_102-108	0.5	56.5	1.5	3.5	1.0	1.0	0.5	0.0	0.0	4.0	2.0	7.0	0.5	1.5	20.5
42_22_5-6cc	0.0	34.5	0.0	0.0	0.0	10.0	0.0	0.0	0.0	26.0	0.0	4.5	0.0	17.5	7.5
32_12_0-5	3.0	28.5	2.0	2.5	5.0	12.5	0.5	0.5	0.0	0.0	10.0	0.0	4.0	0.0	31.5
42_23_33-39	1.0	33.5	0.0	0.5	3.5	2.5	0.0	2.0	0.0	0.0	1.0	8.0	1.0	22.0	25.0
57_16_53-58R2	0.5	32.0	0.5	1.5	2.0	9.0	0.0	2.0	0.0	0.0	0.0	9.5	4.0	25.0	14.0
56_04_130-134	2.0	17.5	1.5	4.5	21.5	5.0	1.0	0.0	0.0	1.0	0.0	21.0	1.0	3.0	21.0
42_18_19-22	5.5	18.0	0.0	5.0	12.0	0.0	0.0	0.0	0.0	0.0	0.0	9.5	1.5	25.5	23.0
57_14_0-4cc	0.5	16.0	1.0	2.0	9.5	0.0	1.0	0.0	0.0	0.0	0.0	8.5	3.0	34.0	24.5
56_04_27-30	3.0	18.0	2.0	7.5	7.5	3.0	1.5	1.0	0.0	0.0	1.0	22.0	1.0	2.5	30.0
57_14_124-130R2	8.5	20.5	2.5	1.5	3.0	1.5	0.5	0.5	0.0	0.0	0.0	10.5	0.5	22.0	28.5
mean	**2.8**	**29.0**	**1.0**	**3.2**	**6.0**	**5.0**	**0.5**	**0.5**	**0.0**	**2.8**	**1.5**	**9.5**	**2.4**	**14.6**	**21.2**

9 *Halimeda* grainstone (hg)

57_07_0-9R2	0.0	4.0	22.0	4.5	7.0	0.0	1.0	2.0	0.0	0.0	2.0	13.0	2.5	27.0	15.0
56_14_38-41	1.5	7.5	30.0	1.0	3.5	1.5	1.0	0.0	0.0	0.0	0.0	8.5	1.5	27.5	16.5
57_07_44-50	2.5	7.0	29.0	1.5	5.0	0.0	2.0	1.0	0.0	0.0	0.0	15.0	0.5	22.0	14.5
42_11_20-27	4.0	3.0	38.5	4.0	12.0	1.5	3.0	0.0	0.0	0.0	3.5	0.0	20.5	0.0	10.0
42_28_33-37	6.5	4.0	38.0	5.5	11.0	1.0	0.0	0.0	0.0	0.0	10.5	0.5	16.5	4.0	2.5
42_11_37-43	3.0	2.0	43.0	6.5	8.0	0.5	0.5	0.0	0.0	0.0	9.5	0.0	23.0	2.5	1.5
42_11_43-50	6.0	1.0	39.5	6.0	6.0	0.5	2.0	0.0	0.0	0.0	17.5	0.5	18.5	2.0	0.5
42_11_27-33	8.0	2.0	29.5	4.5	14.5	2.0	0.5	0.5	0.0	0.0	9.0	0.0	27.5	0.0	2.0
57_07_105-108	4.5	4.0	31.5	3.0	5.5	0.5	0.0	0.0	0.0	0.0	0.0	11.0	25.0	15.0	0.0
57_08_30-35	1.5	6.5	23.0	3.0	5.0	0.5	0.5	0.0	0.0	0.0	0.5	21.0	3.5	34.5	0.5
mean	**3.8**	**4.1**	**32.4**	**4.0**	**7.8**	**0.8**	**1.1**	**0.4**	**0.0**	**0.0**	**5.3**	**7.0**	**13.9**	**13.5**	**6.3**

10 Microbialite (m)

56_07_52-59	0.0	1.0	0.0	3.0	2.0	1.5	0.0	3.5	67.0	0.0	3.0	2.0	11.0	6.0	0.0
mean	**0.0**	**1.0**	**0.0**	**3.0**	**2.0**	**1.5**	**0.0**	**3.5**	**67.0**	**0.0**	**3.0**	**2.0**	**11.0**	**6.0**	**0.0**

11 Caliche (c)

56_08_122-127	0.0	1.0	0.5	2.5	2.5	2.5	0.0	0.0	0.0	56.0	0.0	3.0	3.0	5.0	24.0
56_09_7-18	0.0	0.0	0.5	0.0	1.0	0.0	0.0	0.0	0.0	73.5	0.0	2.0	10.5	5.0	7.5
56_09_75-82	6.0	0.0	4.5	0.5	0.5	0.0	0.0	0.0	0.0	34.5	0.0	14.5	20.5	15.0	4.0
56_15_4-8cc	20.5	0.0	0.0	0.0	0.0	0.0	0.0	0.0	0.0	19.0	13.5	22.5	1.0	23.5	0.0
mean	**6.6**	**0.3**	**1.4**	**0.8**	**1.0**	**0.6**	**0.0**	**0.0**	**0.0**	**45.8**	**3.4**	**10.5**	**8.8**	**12.1**	**8.9**

sample	micrite envelope %	needle cement %	botryoidal cement %	peloidal cement %	microcryst. cement %	syntaxial cement %	blocky cement %	dogtooth cement %	meniscus cement %
32_11_16-22	0.0	5.0	0.0	8.5	0.0	0.0	0.0	0.0	0.0
32_11_32-38	0.0	4.0	0.0	5.0	0.0	0.0	0.0	0.0	0.0
32_12_0-5	0.0	1.5	0.0	2.0	0.5	0.0	0.0	0.0	0.0
32_13_14-18	0.0	4.5	0.5	5.0	15.5	0.0	0.0	0.0	0.0
32_13_24-28	0.0	2.5	0.5	1.0	0.0	0.0	0.0	0.0	0.0
32_19_0-4	0.0	2.5	0.0	3.5	13.0	0.5	0.0	0.0	0.0
33_11_0-5cc	0.0	5.5	0.0	13.0	0.0	0.0	0.5	0.0	0.0
33_12_29-34	0.0	5.0	0.0	2.0	2.0	0.0	0.0	0.0	0.0
33_13_42-46	0.0	1.5	0.0	12.0	1.0	0.0	0.0	0.0	0.0
33_15_17-20	0.0	10.0	0.0	8.5	3.5	0.0	0.0	0.0	0.0
33_16_6-10	0.0	1.0	0.0	0.5	0.0	0.0	0.5	0.0	0.0
33_16_31-37	0.0	2.0	0.0	1.0	1.5	0.0	0.0	0.0	0.0
33_16_59-65	0.0	2.5	0.0	4.0	2.5	0.0	0.0	0.0	0.0
33_16_73-77	0.0	0.0	0.0	0.0	0.0	0.0	0.0	0.0	0.0
33_16_8-13cc	0.0	0.0	0.0	0.0	0.0	0.0	0.0	0.0	0.0
33_18_15-20	0.0	3.5	0.5	5.0	10.5	0.0	0.0	0.0	0.0
33_19_18-25	0.0	4.5	0.0	7.5	0.5	0.0	0.0	0.0	0.0
42_11_20-27	0.5	15.0	0.0	0.0	5.0	0.0	0.0	0.0	0.0
42_11_27-33	4.0	18.0	0.0	0.0	5.5	0.0	0.0	0.0	0.0
42_11_33-37	2.5	8.5	0.0	1.0	4.5	0.0	4.0	0.0	0.0
42_11_37-43	1.0	13.5	0.0	4.5	4.0	0.0	2.5	0.0	0.0
42_11_43-50	1.0	11.5	0.0	3.0	3.0	0.0	2.0	0.0	0.0
42_13_17-18	0.0	0.0	0.0	0.0	0.0	0.0	1.5	0.0	0.0
42_18_19-22	1.5	0.0	0.0	0.0	0.0	0.0	25.0	0.5	0.0
42_18_19-24	0.0	0.0	0.0	0.0	0.0	0.0	12.0	0.0	0.0
42_22_5-6cc	0.0	0.0	0.0	0.0	0.0	0.0	17.5	0.0	0.0
42_23_10-13	4.0	0.0	0.0	0.0	0.0	0.0	36.0	3.0	0.0
42_23_33-39	0.5	0.0	0.5	0.0	0.0	0.0	20.5	1.5	0.0
42_24_22-27	3.5	0.0	0.0	0.0	0.0	0.5	36.5	1.0	0.0
42_25_0-5	7.5	0.0	0.0	0.0	0.0	0.0	13.5	4.0	0.0
42_25_42-48	3.0	0.0	0.0	0.0	0.0	0.0	24.0	2.5	0.0
42_25_54-59	2.0	0.0	0.0	0.0	0.0	0.5	12.5	2.5	0.0
42_27_6-13cc	1.5	0.0	0.0	0.0	0.0	0.0	18.0	1.0	0.0
42_28_0-7	1.5	0.0	0.0	1.5	0.0	0.0	13.0	3.0	0.0
42_11_33-37	2.5	0.0	0.0	0.5	3.0	0.0	23.0	2.5	0.0
55_06_34-37	0.0	3.0	0.0	1.5	5.0	0.0	7.5	0.0	0.0
55_06_41-47	0.0	3.5	0.0	0.0	9.5	0.0	8.0	0.0	0.0
55_07_18-25	2.0	13.5	0.0	0.5	0.5	0.5	18.0	1.0	0.0
55_08_14-17	1.5	26.0	0.5	1.5	0.0	0.5	11.0	0.0	0.0
55_08_38-43	0.5	0.0	0.0	0.0	0.5	0.0	10.5	0.0	0.0
56_01_7-15	0.0	0.0	0.5	4.0	0.0	0.0	15.0	0.0	0.0
56_01_77-80	0.0	2.5	0.0	6.0	5.0	0.0	2.5	0.0	0.0
56_01_100-106	0.0	3.0	0.0	4.5	7.0	0.0	3.0	0.0	0.0
56_02_86-91	1.5	1.0	0.0	2.5	1.5	0.0	0.0	0.0	0.0
56_02_102-108	0.0	0.5	0.0	0.0	0.0	0.0	1.5	0.0	0.0
56_03_0-2	0.0	0.0	0.0	0.0	0.0	0.0	1.0	0.0	0.0
56_03_25-29	0.0	0.0	0.0	0.0	0.0	0.0	0.0	0.0	0.0
56_04_27-30	1.0	0.0	0.0	0.0	0.0	0.0	2.5	0.0	0.0
56_04_130-134	1.0	0.0	0.0	0.0	0.0	0.0	3.0	0.0	0.0
56_05_45-51	0.0	0.0	0.0	0.0	0.0	0.0	6.0	0.0	0.0
56_07_7-8	0.0	0.0	0.0	0.0	0.0	0.0	0.0	0.0	0.0
56_07_42-47	0.0	0.0	0.0	0.0	0.0	0.0	4.0	0.0	0.0
56_07_52-59	0.0	0.5	0.0	10.5	0.0	0.0	6.0	0.0	0.0
56_08_122-127	0.0	0.0	0.0	3.0	0.0	0.0	5.0	0.0	0.0
56_09_7-18	0.0	0.5	0.0	10.0	0.0	0.0	5.0	0.0	0.0
56_09_75-82	0.0	1.5	0.0	18.0	1.0	0.0	15.0	0.0	0.0
56_11_48-51	0.0	0.0	0.0	0.0	0.0	0.0	6.5	0.0	0.0
56_14_38-41	1.0	0.0	0.0	0.5	0.0	0.0	22.0	5.5	0.0
56_15_4-8cc	0.0	0.0	0.0	0.5	0.5	0.0	23.5	0.0	0.0
57_07_44-50	0.0	0.5	0.0	0.0	0.0	0.5	21.5	0.0	0.0
57_07_70-74	2.0	0.0	0.0	0.0	0.0	0.0	26.0	0.0	0.0
57_07_81-86	1.5	1.0	0.0	0.5	3.5	0.0	28.0	1.0	0.0
57_07_105-108	2.5	14.5	8.0	0.0	0.0	0.0	15.0	0.0	0.0
57_07_127-130	1.5	0.5	0.0	1.5	0.0	0.0	34.5	1.0	0.0
57_07_0-9R2	1.5	0.0	0.0	1.0	0.0	0.0	25.5	1.5	0.0
57_08_13-19	3.0	0.0	0.0	0.0	0.0	0.0	33.5	3.0	5.5

57_08_30-35	3.5	0.0	0.0	0.0	0.0	0.0	26.0	2.5	6.0
57_10_0-5	2.5	0.0	0.0	0.5	0.0	0.0	22.0	3.0	6.0
57_10_20-24	1.5	0.0	0.0	0.0	0.0	0.0	28.0	2.5	4.0
57_10_44-50	2.5	0.0	0.0	0.0	0.0	0.0	24.0	4.0	6.0
57_10_76-80	2.0	0.0	0.0	1.0	24.0	0.0	23.5	1.0	0.0
57_10_95-101	2.0	0.0	0.0	0.0	0.0	0.0	18.0	1.0	2.0
57_10_3-7cc	1.0	0.0	0.0	0.0	2.0	0.0	18.0	0.5	0.0
57_11_1-4	2.0	0.0	0.0	0.0	0.0	0.0	30.5	1.0	1.0
57_11_40-43	0.0	0.0	0.0	0.0	6.0	0.0	25.0	7.5	0.0
57_12_8-11	1.5	0.0	0.0	0.0	0.0	0.5	33.0	2.5	0.0
57_12_34-38	0.0	0.0	0.0	0.0	0.0	0.5	37.0	0.5	0.0
57_12_0-6cc	0.0	0.0	0.0	0.0	0.0	0.0	25.6	1.8	0.0
57_13_10-15	1.0	0.0	0.0	0.0	0.0	0.0	31.5	2.5	0.0
57_13_40-45	1.5	0.0	0.0	0.0	3.5	0.0	28.0	2.5	0.0
57_14_9-15	1.0	0.0	0.0	0.0	0.0	0.0	17.0	2.0	0.0
57_14_27-31	2.0	0.0	0.0	0.0	0.0	0.0	21.5	1.5	0.0
57_14_0-5R2	0.0	0.0	0.0	0.0	0.0	0.0	13.0	0.5	0.0
57_14_22-29R2	1.5	0.0	0.0	0.0	0.0	0.0	24.5	3.0	0.0
57_14_47-52R2	0.5	0.0	0.0	0.0	0.0	0.0	26.5	2.0	0.0
57_14_81-86R2	0.0	0.0	0.0	2.0	0.0	0.0	10.5	1.0	0.0
7_14_124-130R	0.5	0.0	0.0	0.0	0.0	0.0	18.5	3.5	0.0
57_14_0-4cc	2.5	0.0	0.0	0.5	0.0	0.0	30.0	4.0	0.0
57_15_3-8	1.0	0.0	0.0	0.0	0.0	0.0	23.5	3.0	0.0
57_15_39-42	0.0	0.0	0.0	0.0	0.0	0.0	22.0	2.0	0.0
57_15_98-103	0.0	0.0	0.0	2.0	9.0	0.0	30.5	1.5	0.0
57_15_4-9R2	0.5	0.0	0.0	1.0	0.0	0.0	24.0	1.5	0.0
57_15_42-47R2	0.0	0.0	0.0	0.5	2.5	0.0	27.5	2.5	0.0
57_15_73-74R2	0.0	0.0	0.0	2.0	0.5	0.0	18.0	2.0	0.0
57_16_20-28	2.0	0.0	0.0	2.0	0.0	0.0	31.0	5.5	0.0
57_16_44-55	1.5	0.0	0.0	3.0	0.0	1.0	26.5	7.0	0.0
57_16_118-124	2.5	0.0	0.0	2.5	0.0	0.0	28.5	3.5	0.0
57_16_136-142	2.0	0.0	0.0	0.0	1.0	0.0	25.5	2.5	0.0
57_16_19-23R2	1.5	0.0	0.0	3.5	0.0	0.0	27.5	1.5	0.0
57_16_53-58R2	1.5	0.0	0.0	2.5	0.0	0.0	22.5	2.5	0.0

sample	depth mbSL	QTZ rel wt %	ARA rel wt %	HMC rel wt %	LMC rel wt %	d13C ‰	d18O ‰
32_11_16-22	109.89	0.0	77.0	20.7	2.3	2.19	0.06
32_11_32-38	110.05	0.0	77.3	22.7	0.0	2.62	0.23
32_12_0-5	111.73	0.0	83.1	16.9	0.0	3.34	0.68
32_13_14-18	113.86	0.0	94.8	4.3	0.9	1.34	-1.06
32_13_24-28	113.96	0.0	53.1	44.9	2.0	3.88	0.59
32_19_0-4	124.72	0.0	71.0	29.0	0.0	2.10	-0.34
33_11_0-5cc	107.08	0.0	60.0	38.6	1.4	3.48	0.72
33_12_29-34	107.42	0.0	98.0	2.0	0.0	2.05	-0.53
33_13_42-46	108.54	0.0	59.7	37.2	3.1	2.96	0.23
33_15_17-20	111.29	0.0	55.3	43.0	1.8	2.57	0.18
33_16_6-10	112.18	0.0	69.3	29.4	1.2	3.69	0.80
33_16_31-37	112.44	0.0	58.3	38.0	3.7	3.80	0.80
33_16_59-65	112.72	1.6	47.0	49.4	1.9	3.81	0.66
33_16_73-77	112.85	0.0	58.3	39.7	2.0	3.82	0.72
33_16_8-13cc	113.58	0.0	85.9	12.5	1.6	2.96	0.16
33_18_15-20	113.78	0.0	0.0	67.2	32.8		
33_19_18-25	115.32	0.0	81.7	17.2	1.1	2.02	-0.12
42_11_20-27	66.24	0.0	92.5	2.7	4.8	2.08	-1.20
42_11_27-33	66.3	0.0	96.0	1.8	2.2	4.29	-0.23
42_11_33-37	66.35	0.0	86.3	3.9	9.8	2.11	-1.53
42_11_37-43	66.4	0.0	93.8	2.0	4.2	3.57	-0.54
42_11_43-50	66.47	0.0	88.8	2.6	8.6	0.79	-1.85
42_13_17-18	68.48	0.0	68.7	0.3	31.0	-1.62	-3.74
42_18_19-22	76.01	0.0	15.7	1.0	83.3	-0.85	-4.59
42_18_19-24	76.02	1.6	26.7	0.0	71.7	-0.62	-3.90
42_22_5-6cc	84.75	1.3	18.6	1.0	79.2	-0.36	-4.36
42_23_10-13	84.92	0.0	0.0	0.0	100.0	-1.75	-4.71
42_23_33-39	85.16	0.0	10.8	0.0	89.2	-3.79	-4.86
42_24_22-27	86.26	0.0	7.0	0.0	93.0	-2.07	-5.14
42_25_0-5	87.53	0.0	0.0	0.0	100.0	-1.44	-4.91
42_25_42-48	87.95	1.3	0.0	0.0	98.7	-4.89	-4.69
42_25_54-59	88.07	0.0	0.0	0.0	100.0	-1.49	-5.00
42_27_6-13cc	92.91	0.0	9.3	0.0	90.7	-2.40	-4.97
42_28_0-7	93.04	0.0	22.5	0.0	77.5	-2.14	-4.51
42_28_33-37	93.35	0.0	10.0	0.0	90.0	-1.15	-4.34
55_06_34-37	103.45	0.0	50.2	0.0	49.8	0.79	-2.81
55_06_41-47	103.53	0.0	31.9	0.0	68.1	0.08	-4.19
55_07_18-25	106.81	0.0	81.1	0.3	18.6	2.65	-1.22
55_08_14-17	109.75	0.0	63.4	0.0	36.6	2.00	-1.64
55_08_38-43	110	0.0	47.2	0.0	52.8	0.45	-3.62
56_01_7-15	82.4	0.0	61.1	37.4	1.5	3.52	0.07
56_01_77-80	83.08	0.0	83.0	16.5	0.5	2.04	-1.09
56_01_100-106	83.32	1.2	77.1	20.7	0.9	3.35	0.13
56_02_86-91	86.18	0.0	75.9	15.7	8.3	2.37	-0.49
56_02_102-108	86.35	0.0	43.3	23.2	33.5	1.16	-0.73
56_03_0-2	87.3	2.2	21.0	31.1	45.8	-1.21	-1.76
56_03_25-29	87.56	0.0	12.6	0.0	87.4	-2.72	-3.34
56_04_27-30	90.58	0.0	13.8	0.0	86.2	-2.82	-3.78
56_04_130-134	91.61	2.6	16.8	0.0	80.7	-1.29	-3.66
56_05_45-51	93.78	2.2	11.7	0.0	86.1	-0.77	-4.22
56_07_7-8	99.37	0.0	0.0	0.0	100.0	-0.49	-3.68
56_07_42-47	99.74	0.0	30.7	0.0	69.3	0.66	-3.43
56_07_52-59	99.85	3.6	24.7	46.2	25.5	2.85	-0.98
56_08_122-127	102.54	0.0	26.0	37.3	36.7	1.95	-1.64

56_09_7-18	104.41	2.8	19.8	38.5	38.8	2.34	-1.88
56_09_75-82	105.08	0.0	46.9	37.7	15.5	2.96	-0.36
56_11_48-51	110.79	0.0	46.7	0.0	53.3	1.26	-3.59
56_14_38-41	116.69	0.0	28.9	0.0	71.1	0.65	-4.10
56_15_4-8cc	119.43	0.0	66.5	10.5	23.0	1.78	-2.38
57_07_44-50	60.45	0.0	17.3	0.0	82.7	-0.94	-4.40
57_07_70-74	60.7	0.0	23.3	3.5	73.2	-3.67	-4.01
57_07_81-86	60.82	0.0	72.0	0.0	28.0	0.41	-2.74
57_07_105-108	61.05	0.0	82.5	0.0	17.5	1.75	-2.19
57_07_127-130	61.27	0.0	65.9	0.0	34.1	0.62	-2.65
57_07_0-9R2	61.5	0.0	25.9	0.0	74.1	-2.12	-4.26
57_08_13-19	63.14	0.0	9.2	0.0	90.8	-4.30	-5.06
57_08_30-35	63.31	0.0	14.0	0.0	86.0	-4.29	-5.03
57_10_0-5	66.51	0.0	2.7	0.0	97.3	-3.94	-5.18
57_10_20-24	66.7	0.0	2.9	0.0	97.1	-2.79	-5.00
57_10_44-50	66.95	0.8	2.8	0.0	96.4	-2.32	-4.92
57_10_76-80	67.26	0.0	4.1	0.0	95.9	-2.05	-4.89
57_10_95-101	67.46	0.0	4.4	0.0	95.6	-1.94	-4.88
57_10_3-7cc	68.63	0.0	3.8	0.0	96.2	-1.25	-4.77
57_11_1-4	68.71	1.9	0.0	0.0	98.1	-3.39	-4.95
57_11_40-43	69.1	0.0	5.6	0.0	94.4	-1.89	-5.05
57_12_8-11	71.78	0.0	0.0	0.0	100.0	-0.89	-4.77
57_12_34-38	72.05	0.0	5.4	0.0	94.6	-0.54	-4.76
57_12_0-6cc	74.65	0.0	0.0	0.0	100.0	-0.33	-4.80
57_13_10-15	74.81	0.0	0.0	0.0	100.0	-0.55	-4.82
57_13_40-45	75.11	0.0	0.0	0.0	100.0	-6.44	-4.74
57_14_9-15	76	0.0	0.0	0.0	100.0	-6.51	-4.81
57_14_27-31	76.17	0.0	5.0	0.0	95.0	-7.99	-5.08
57_14_0-5R2	76.29	0.0	0.0	0.0	100.0	-6.32	-4.61
57_14_22-29R2	76.52	0.0	4.3	0.0	95.7	-6.11	-4.55
57_14_47-52R2	76.76	1.2	0.0	0.0	98.8	-6.33	-4.72
57_14_81-86R2	77.1	0.0	0.0	0.0	100.0	-6.06	-4.88
57_14_124-130R2	77.53	1.4	0.0	0.0	98.6	-4.12	-4.54
57_14_0-4cc	78.06	1.7	0.0	0.0	98.3	-4.53	-4.67
57_15_3-8	78.15	0.7	2.8	0.0	96.5	-6.26	-5.00
57_15_39-42	78.49	0.0	0.0	0.0	100.0	-4.49	-4.65
57_15_98-103	79.09	1.5	0.0	0.0	98.5	-4.65	-4.93
57_15_4-9R2	79.19	0.0	0.0	0.0	100.0	-4.77	-4.94
57_15_42-47R2	79.57	0.0	0.0	0.0	100.0	-4.11	-4.74
57_15_73-74R2	79.86	0.0	0.0	0.0	100.0	-5.25	-5.06
57_16_20-28	81.32	0.9	0.0	0.0	99.1	-3.31	-4.62
57_16_44-55	81.58	0.0	4.6	0.0	95.4	-3.09	-4.88
57_16_118-124	82.29	0.0	0.0	0.0	100.0	-2.69	-4.89
57_16_136-142	82.47	0.0	0.0	0.0	100.0	-3.95	-4.83
57_16_19-23R2	82.77	0.0	0.0	0.0	100.0	-2.89	-4.73
57_16_53-58R2	83.11	0.0	60.2	0.0	39.8	-2.69	-4.67

Sedimentology

	coral	corr alga	Halimeda	mollusk	for benth	for encr	echino	peloid	primporo	secporo	matrix	microbia	caliche	depth	QTZ	ARA	LMC	HMC	d13C	d18O	mar cem	met cem
coral		0.468	0.017	0.019	0.000	0.439	0.252	0.018	0.000	0.000	0.188	0.440	0.307	0.004	0.412	0.039	0.011	0.023	0.068	0.011	0.000	0.042
corr alga	-0.073		0.001	0.763	0.696	0.000	0.506	0.675	0.064	0.795	0.029	0.317	0.181	0.607	0.693	0.115	0.076	0.207	0.125	0.166	0.041	0.409
Halimeda	**-0.239**	**-0.330**		0.022	0.008	0.012	0.018	0.113	0.072	0.411	0.042	0.528	0.156	0.000	0.167	0.000	0.027	0.040	0.159	0.494	0.005	0.328
mollusk	**-0.235**	-0.031	**0.229**		0.000	0.447	0.000	0.252	0.810	0.588	0.946	0.862	0.028	0.910	0.589	0.047	0.223	0.325	0.309	0.381	0.822	0.030
for benth	**-0.416**	-0.040	**0.262**	**0.361**		0.562	0.042	0.001	0.363	0.051	0.685	0.425	0.016	0.083	0.695	0.613	0.214	0.026	0.610	0.182	0.114	0.980
for encr	-0.078	**0.351**	**-0.250**	0.077	-0.059		0.413	0.580	0.964	0.025	0.345	0.773	0.482	0.007	0.859	0.477	0.198	0.060	0.251	0.065	0.916	0.061
echino	-0.116	-0.067	**0.235**	**0.426**	**0.204**	-0.083		0.618	0.998	0.246	0.844	0.472	0.074	0.768	0.476	0.454	0.982	0.088	0.779	0.996	0.652	0.167
peloid	**-0.236**	0.043	-0.160	0.116	**0.339**	0.056	-0.050		0.463	0.871	0.336	0.147	0.174	0.141	0.723	0.287	0.367	0.933	0.619	0.592	0.054	0.794
primporo	**0.402**	-0.186	0.181	0.024	-0.092	0.005	0.000	-0.074		0.000	0.245	0.906	0.318	0.030	0.145	0.000	0.000	0.108	0.000	0.000	0.000	0.002
secporo	**-0.350**	0.026	-0.083	0.055	0.196	**-0.225**	0.117	0.016	**-0.420**		0.002	0.316	0.320	0.000	0.927	0.000	0.000	0.000	0.000	0.000	0.000	0.000
matrix	-0.133	**-0.218**	**-0.204**	0.007	-0.041	0.095	-0.020	0.097	-0.117	**-0.308**		0.284	0.474	0.000	0.567	0.124	0.013	0.001	0.056	0.000	0.001	0.000
microbia	-0.078	-0.101	-0.064	-0.018	-0.081	-0.029	-0.073	0.146	0.012	-0.101	-0.108		0.780	0.463	0.000	0.831	0.402	0.013	0.245	0.316	0.547	0.447
caliche	-0.103	-0.135	-0.143	**-0.220**	**-0.241**	-0.071	-0.180	-0.137	-0.101	-0.100	-0.072	-0.028		0.155	0.010	0.829	0.356	0.005	0.204	0.334	0.803	0.242
depth	**0.287**	0.052	**-0.387**	-0.011	-0.174	**0.269**	0.030	0.148	0.217	**-0.443**	**0.382**	0.074	0.143		0.834	0.000	0.000	0.000	0.000	0.000	0.102	0.000
QTZ	-0.083	-0.040	-0.139	-0.055	0.040	-0.018	0.072	-0.036	-0.147	0.009	-0.058	**0.459**	**0.255**	0.021		0.047	0.437	0.087	0.687	0.817	0.323	0.656
ARA	**0.206**	-0.159	**0.371**	0.199	-0.051	0.072	0.076	-0.107	**0.479**	**-0.564**	0.155	-0.022	-0.022	**0.349**	-0.199		0.000	0.001	0.000	0.000	0.000	0.000
LMC	**-0.253**	0.178	**-0.221**	-0.123	0.125	-0.130	0.002	0.091	**-0.448**	**0.645**	**-0.247**	-0.085	-0.093	**-0.502**	0.079	**-0.931**		0.000	0.000	0.000	0.000	0.000
HMC	**0.227**	-0.127	**-0.206**	-0.099	**-0.222**	0.189	-0.172	-0.009	0.162	**-0.491**	**0.320**	**0.248**	**0.280**	**0.573**	0.172	**0.319**	**-0.642**		0.000	0.000	0.005	0.000
d13C	0.183	-0.154	0.142	0.103	-0.052	0.116	0.028	-0.050	**0.375**	**-0.508**	0.192	0.117	0.128	**0.543**	-0.041	**0.768**	**-0.860**	**0.621**		0.000	0.000	0.000
d18O	**0.253**	-0.139	0.069	0.089	-0.134	0.185	0.000	-0.054	**0.403**	**-0.665**	**0.360**	0.101	0.098	**0.591**	-0.023	**0.805**	**-0.947**	**0.770**	**0.860**		0.000	0.000
mar cem	**0.517**	**-0.205**	**0.281**	-0.023	-0.159	-0.011	0.046	-0.194	**0.400**	**-0.473**	**-0.320**	0.061	0.025	0.164	-0.100	**0.556**	**-0.557**	**0.281**	**0.495**	**0.510**		0.000
met cem	**-0.204**	0.084	-0.099	**-0.217**	0.003	-0.188	-0.139	0.026	**-0.305**	**0.594**	**-0.480**	-0.077	-0.118	**-0.573**	-0.045	**-0.643**	**0.735**	**-0.554**	**-0.659**	**-0.777**	**-0.364**	